A high-resolution carbon-isotope record of the Turonian stage (93.9 – 89.8 Ma) correlated to a siliciclastic basin fill: implications for mid-Cretaceous sea-level change

D. Uličný [1], D. Gröcke [2], S. Čech [3], J. Laurin [1], I. Jarvis [4], K. Olde [4], J. Trabucho-Alexandre [2], L. Švábenická [4], N. Pedentchouk [5] , T. Matys-Grygar [6]

[1] Institute of Geophysics, Academy of Sciences of the Czech Republic, 141 31 Prague, Czech Republic (ulicny@ig.cas.cz)

[2] Department of Earth Sciences, Durham University, Durham DH1 3LE, UK

[3] Czech Geological Survey, 118 21 Prague, Czech Republic

[4] School of Geography, Geology and Environment, Kingston University London, Kingston upon Thames KT1 2EE, UK

[5] School of Environmental Sciences, University of East Anglia, Norwich NR4 7TJ, UK

[6] Institute of Inorganic Chemistry, Academy of Sciences of the Czech Republic, Husinec-Řež 1001, 250 68 Řež, Czech Republic

ABSTRACT

A basin-scale record of high-frequency transgressive-regressive (T-R) fluctuations of Turonian age in the Bohemian Cretaceous Basin, Central Europe, has previously been interpreted as being significantly influenced by short-term eustasy. Here, nearshore siliciclastic strata in two separate sub-basins are correlated to a multi-stratigraphic dataset from a new research core (Bch-1) drilled in offshore marine sediments of the central basin. A high-resolution $\delta^{13}C_{org}$ record from Bch-1 is presented along with major- and minor-element proxies, TOC, carbonate contents, terrestrial to marine palynomorph ratios, and detailed macro- and microfossil biostratigraphy. The 400 m thick Turonian through Lower Coniacian interval permits correlation to the highest-resolution C-isotope curves available: all carbon-isotope events demonstrated by $\delta^{13}C_{carb}$ studies in the British Chalk, NW Germany and other reference sections in Europe are recognised in the $\delta^{13}C_{org}$ curve from Bch-1.

A number of short-term, basin-wide regressions in the Bohemian Cretaceous Basin show a recurrence interval of 100 kyr or less. This is an order of magnitude shorter than the timing of sea-level falls inferred from the New Jersey margin and the Apulian platform, interpreted to having been driven by glacioeustacy. The small magnitude of the Bohemian Basin sea-level falls, typically < 40 m, indicates that the 2.4 Myr period suggested by others to generate 3rd-

order cycles, is too long to be the principal cycle generating unconformities in tectonically active basins, where the rate of eustatic fall must exceed the subsidence rate. Unconformities in low-accommodation settings such as passive margins must represent amalgamated records of multiple cycles of sea-level fluctuations of 100 kyr scale, recognizable only in high-resolution datasets from expanded basinal sections.

Comparison of the $\delta^{13}C$ excursions to the interpreted sea-level record fails to yield conclusive results regarding potential causal links. A long-term 'background' $\delta^{13}C$ cycle shows a duration close to the 2.4 Myr long-eccentricity cycle, and shorter-term (1 Myr scale) highs and lows in $\delta^{13}C$ appear to broadly correspond to intervals characterized by more pronounced short-term sea-level highs and lows, respectively. However, on the scale of intermediate to short-term $\delta^{13}C$ fluctuations, no systematic relationship between $\delta^{13}C$ and sea-level change can be demonstrated.

1. Introduction

The Late Cenomanian through Early Coniacian included a global long-term sea-level maximum near the Cenomanian-Turonian (C-T) boundary, as well as a long-term sea-level low in the Middle Turonian (e.g. Haq et al., 1988; Kominz et al., 2008). Superimposed, high-frequency relative sea-level changes within this time interval, and other periods of mid-Cretaceous greenhouse time, with recurrence intervals within the Milankovitch band, have been reported from many basins (Plint, 1991; Gardner, 1995; Immenhauser & Matthews, 2004; Laurin & Uličný, 2004; Immenhauser, 2005; Laurin & Sageman, 2007; Varban & Plint, 2008; Uličný et al., 2009; Zhu et al., 2012), and invoked in stratigraphic forward models (Somme et al., 2008). The exact timing and duration of such fluctuations, however, have not been agreed and will require high-resolution inter-basinal correlation. The importance of this task is underlined by the current debate on potential greenhouse glacioeustasy during the Cretaceous (Miller et al., 2003, 2005; Moriya et al., 2007; Bornemann et al., 2008; Kominz et al., 2008; Ando et al., 2009; Flögel et al., 2011).

Glacioeustacy is particularly controversial for the Turonian, which represents arguably the warmest climate for the entire period (Bice et al., 2003; Friedrich et al., 2012). Significant uncertainties in biostratigraphic dating, the long duration of hiatuses in many key sections, as well as the fact that the duration of the suspected high-frequency sea-level fluctuations is below biostratigraphic zonal resolution, have so far prevented correlation of low-order Milankovitch band sea-level events between basins with any certainty.

Carbon-isotope chemostratigraphy has been developed as a powerful correlation tool in the Cretaceous and other intervals of geological history (e.g. Scholle & Arthur, 1980; Gale et al., 1993, Jarvis et al., 2006), with a resolution well below limits of biozones and a unique capability to link marine and terrestrial records (Gröcke et al., 1999, 2002; Hesselbo & Pienkowski, 2011; Takashima et al., 2011). Due to the short mixing time of carbon in the ocean-atmosphere system, in the order of 10^3 yr (Siegenthaler & Sarmiento, 1993), correlation of $\delta^{13}C$ variations among sites on kyr time scales has been demonstrated, to a point where it has been suggested that chemostratigraphy might substitute for biostratigraphy in some intervals of the geological record (e.g. Herrle et al., 2004).

Causal links between the carbon stable-isotope fluctuations and eustatic sea-level variation have been suggested, with a positive correlation between sea level and $\delta^{13}C$ initially being proposed based on low-resolution studies focusing on the long-term maximum flooding near the Cenomanian-Turonian boundary (Scholle & Arthur 1980). An underlying assumption is that an increase in organic C production and deposition will result in an increase in $\delta^{13}C$ value of the remaining dissolved C in the oceanic reservoir. Later work, utilizing progressively higher-resolution datasets, resulted in interpretations of the covariance between global sea level and carbon-isotope events (CIEs) on a Myr timescale (Mitchell et al., 1996; Gale, 1996; Jarvis et al., 2002, 2006), and potentially even 100 kyr (Uličný et al., 1997). Other authors have suggested, however, that some positive CIEs in the Cretaceous correlate to relative sea-level falls (Gröcke et al., 1999, 2006), including those of the Middle and Late Turonian (Voigt, 2000; Wiese & Voigt, 2002), with Bornemann et al. (2008) and Takashima (2010) explicitly interpreting the positive $\delta^{13}C$ excursion of the late Middle Turonian 'Pewsey' positive CIE to correlate to a short-term glacioeustatic fall.

Quantitative modelling of carbon burial during sea-level rise can, under certain conditions, simulate limited positive excursions in $\delta^{13}C$ (Bjerrum et al., 2006), but although sea-level rise and organic-C deposition may react to the same forcing, they need not have a direct causal link. Recent studies of Mesozoic and Cenozoic datasets that demonstrate orbital-driven, climatic control of $\delta^{13}C$ fluctuations (Cramer et al., 2003; Pälike et al., 2006; Voigt et al., 2007; Giorgioni et al., 2012) do not interpret direct links with sea-level change.

In case that a eustatic component of base-level change can be interpreted from a transgressive-regressive (T-R) record of a particular sedimentary basin fill, then a comparison of the T-R history to the $\delta^{13}C$ record in the same basin will contribute significantly to understanding of the relationships between sea-level change and the carbon

cycle. Most published Turonian $\delta^{13}C$ curves come from pelagic or hemipelagic successions that lack direct physical correlation to shallow-water, nearshore successions that provide records of shoreline movement through time. Correlation to presumed global eustatic sea-level has typically been made using either the Haq et al. (1988) cycle charts (e.g. Stoll & Schrag, 2000; Voigt, 2000), or by comparison with shallow-water records studied elsewhere (e.g. Jarvis et al., 2006 referring to Sahagian et al., 1996). One notable exception is that of Gale (1996) who derived the sea-level trends from stratal geometries of the Chalk from where his $\delta^{13}C$ record originated.

Demonstrating a direct record of net eustatic change is not possible in nearshore records (Burton et al., 1987) because the sea-level signal in the stratigraphic record is altered by the effects of tectonic subsidence, sediment supply, and the intrinsic dynamics of depositional systems. Studies based on large datasets with high stratigraphic resolution have shown, however, that it is possible to differentiate tectonic and supply-driven changes in stratal geometries from those most likely driven by eustasy (e.g. Varban & Plint, 2008). In order to accomplish this goal, it is necessary to carefully evaluate stratal geometries using regional, basin-scale, three-dimensional (3D) datasets. In such a case it is possible to take advantage of the fact that tectonically subsiding basins offer expanded records with fewer, or less extensive, unconformities than carbonate platforms, shallower-water pelagic settings, or up-dip parts of passive margins.

Previous research in the Bohemian Cretaceous Basin of Central Europe (Uličný et al., 2009) has invoked eustasy forcing as a partial control on the transgressive-regressive history of siliciclastic deltaic and nearshore systems. Based on stratal geometries, temporal and spatial variations in tectonic subsidence and supply rate were identified in the basin fill, and proximal nearshore facies were correlated to distal offshore hemipelagic strata (Laurin & Uličný, 2004; Uličný et al., 2009).

The primary aim of the present paper is to compare regional T-R histories that contain an interpreted short-term eustatic component, with a high-resolution organic matter carbon-isotope ($\delta^{13}C_{org}$) record, and to evaluate the potential for detailed correlations in Europe and worldwide. Additionally, the role of stratigraphic resolution in inferring relationships between sea-level change and $\delta^{13}C$ in this and other datasets are addressed. Finally, the timing of $\delta^{13}C$ fluctuations and their relationship to orbital frequencies are briefly discussed.

2. Data and methods

A new research core was drilled in 2010 through offshore marine sediments of late Cenomanian – early Coniacian age in the Bohemian Cretaceous Basin (Bch-1, Fig. 1), at Běchary, east-central Czech Republic (see Appendix 1 for details). Fluctuations in $\delta^{13}C_{org}$, major- and minor-element proxies, palynological assemblages, and petrological composition, documented in the core, were correlated to the depositional histories of two depocentres of the Basin: the Lužice-Jizera sub-basin in the NW; and the Orlice-Žďár sub-basin in the SE (Fig. 1B). The two depocentres were part of the same seaway developed along the reactivated Elbe Fault System, but their deposits were sourced from different blocks uplifted along separate faults. As a consequence, the subsidence rates and clastic input fluxes differ.

A basin-scale correlation grid was developed based on well-log data (gamma-ray, resistivity, neutron porosity logs) from around 1000 boreholes, in most cases supplemented by either archive descriptions of cores or study of cores by the authors and, where possible, calibrated by outcrop sedimentology and gamma-ray logging. For the NW depocentre, details of the sequence-stratigraphic approach and types of genetic sequences were described by Uličný et al. (2009). Data from the SE depocentre, presented here, were treated in an analogous way. Genetic sequences, bounded by maximum transgressive surfaces, form a hierarchy of nested, as a response to relative sea-level changes. Transgressive and regressive (T-R) histories are derived from tracking the *maximum regressive facies* within composite genetic sequences and *maximum transgressive surfaces* separating the sequences, i.e. they are based on the genetic sequence concept of Galloway (1989), not the T-R sequence in the sense of Embry (1995).

Correlation of the two separate sub-basins may be considered to be halfway between intra- to inter-basinal. Importantly, interpretations of T-R history on a sub-basin-scale were based on an evaluation of 3D geometries within a detailed well-log correlation framework. This approach permits a qualitative to semi-quantitative assessment of temporal changes in subsidence and supply rates (Laurin & Uličný, 2004; Uličný et al., 2009). Comparison of the two T-R records permits an interpretation of: (a) eustatic forcing / influence in case of synchronous events; and (b) relative differences in clastic supply and tectonic-driven accommodation evolution through time in case of strongly different T-R histories. Compared to Uličný et al. (2009), some correlations in the NW sub-basin were revised based on new data.

A particular strength of the Bohemian Cretaceous Basin stratigraphic dataset is the linkage of the physical stratigraphy to a detailed biostratigraphic framework (cf. Čech, 1989; Laurin & Uličný, 2004; Uličný et al., 2009, b). Macrofossil and calcareous nannofossil data from the Bch-1 core have been combined with first occurrences (FO) and acmes of key Turonian macrofossil taxa from correlative cores and outcrops. The stratigraphic resolution of the correlations, which employ densely spaced well logs, is typically in the order of 1 – 5 m (10 – 50 kyr, see below). In the Turonian, 12 macrofossil datum levels are recognized (Fig. 2), of which 7 are identical with those used by Jarvis et al. (2006) to constrain their European reference carbon-isotope stratigraphy. In addition, 4 nannofossil markers were used to determine the length of the hiatus at the C-T boundary. All correlations of events in the $\delta^{13}C_{org}$ curve were corroborated against the biostratigraphic markers in order to avoid miscorrelations arising from simple 'wiggle-matching'.

The $\delta^{13}C_{org}$ data presented here (Figs 2, 3) are based on analysis of bulk organic matter, which is dominantly of marine origin. Previous carbonate-based $\delta^{13}C$ data from the Bohemian Cretaceous Basin show diagenetic alteration in some intervals of lower primary carbonate content (Uličný et al., 1993), and thus $\delta^{13}C_{org}$ was considered to be a more reliable carrier of primary signal through the entire study interval. Analytical reproducibility of replicate samples was on average ±0.15‰. Total organic carbon (TOC) contents of the insoluble residues were determined as part of the $\delta^{13}C_{org}$ analytical protocol and were recalculated to bulk-rock values using carbonate contents derived from Ca values determined by ICP atomic emission spectrometry (ICP-AES; cf. Jarvis et al., 2011).

Potential distortion of the marine $\delta^{13}C_{org}$ signal caused by varying influx of terrestrial organic matter was monitored with the aid of quantitative palynology. In selected samples, the relative contribution of terrigenous versus aquatically derived organic matter was determined using *n*-alkane ratios (TAR_{HC}; cf. Meyers, 1989 and references therein). The ratio of terrestrial to marine palynomorphs (T:M) and Si/Al, Ti/Al and Zr/Al ratios provide siliciclastic-flux proxies, which are used to complement the T-R interpretations.

Estimated timing of major changes in depositional history and in $\delta^{13}C_{org}$ was based on a linear interpolation of ages from Ogg & Hinnov (2012), with an alternative age assignment of the base of the Middle Turonian discussed below. Details of laboratory procedures and numerical data are reported in Appendix 1.

3. Turonian depositional history

3.1. The Bch-1 core: facies, T:M ratios and elemental proxies

The facies succession of the Turonian and Lower Coniacian in Bch-1 is typical of the central part of the Bohemian Cretaceous Basin (cf. Klein et al., 1982; Čech, 1989; Čech et al., 2011). The predominant lithofacies in the Bch-1 core (Fig. 2) are marlstones with a varying proportion of quartz silt (maxima near 360 – 380 m and 140 – 220 m) and a mean $CaCO_3$ content of ~ 25%, reaching over 50% between 140 and 250 m. The carbonate is generally micritic, locally containing scattered mm-size bioclasts, with significant spar occurring in horizons with concretionary cementation. TOC values range between 0.2 and 0.4 wt% below 220 m depth, and are generally 0.4 – 0.7 wt% above. All lithologies are typically strongly bioturbated, with ichnotaxa indicative of a distal *Cruziana* ichnofacies *sensu* MacEachern et al. (2010). Lower to Middle Turonian marlstones between 359 and 385 m are rich in sponge spicules (mainly calcified silica sponges). Burrowed omission surfaces, overlain by glauconite-rich marlstones with phosphatized bioclasts and locally enriched in silt- to fine sand-grade quartz grains, occur at two well-defined levels: 359 and 402 m. These may be correlated basinwide, accompanied by several less regionally extensive glauconite-rich zones, mainly in the uppermost Turonian (Fig. 2 and Fig. S1).

The Si/Al ratio shows two long-term maxima in the Turonian: 160 – 220 m and 360 – 380m, with higher-frequency fluctuations superimposed in the regions of both high and low long-term values. Ti/Al and Zr/Al ratios show analogous patterns, indicating that the Si/Al high between 359 and 385m represents primarily a terrestrial input signal, not the migration of silicifica during diagenesis (Fig. S2). In most of the core, marine palynomorphs strongly predominate over terrestrial elements, with two broad peaks of the T:M ratio near 350 m depth and between 160 and 220 m (Fig. 2), where in several samples terrestrial palynomorphs reach over 25 per cent.

The entire Turonian at the Bch-1 site was characterised by deposition in a fully marine offshore setting, mostly well below storm wave base, with oxygenated bottom conditions. Locally preserved silt and/or silt-sized skeletal laminae suggest intermittent, distal effects of storm events during some periods of deposition, but bioturbation has destroyed signs of primary depositional fabrics in the cored facies. Average compacted sedimentation rates for the Middle and Upper Turonian range from 8.5 to 9 cm/kyr, depending on the choice of age for the base of the *C. woollgari* Zone [92.9 Ma in Ogg et al. (2012) vs. 93.1 Ma based on an estimated 800 kyr duration of Lower Turonian in Sageman et al. (2006) and Voigt et al.

(2008b)]. The presence of several condensed horizons as well as fluctuating T:M and elemental proxies indicate that the depositional setting experienced fluctuations in sedimentation rate, mainly due to changing shore proximity. In order to decipher details of depositional history on time scales shorter than several Myr, however, direct correlation to the nearshore facies is necessary.

Below, the principal transgressive-regressive events of the basin history, as interpreted from the NW and SE nearshore depocentres, are reviewed in stratigraphic order, and linked to the Bch-1 succession.

3.2. Genetic sequences and evolution of basin filling

3.2.1. Nearshore depositional systems and derivation of T-Rmax diagrams

The style of basin filling during the Turonian and early Coniacian was dominated by repeated progradation of coarse-grained deltas and adjoining shorefaces, affected by redistribution of clastics by strong along-shore currents of tidal origin (Uličný, 2001; Mitchell et al., 2010). The resulting basic building blocks of stratigraphy are sheet-like sandstone bodies, lobate in plan view, typically between 10 and 25 m thick, but in some cases reaching up to 100 m in thickness in the case of deep-water Gilbert-type deltas (Uličný et al., 2009). Offshore and along-shore transport of suspended load by hypopycnal plumes, affected by the axial currents, was probably an important factor in grain-size partitioning between the sand-dominated proximal and mud- to marl-dominated distal parts of the basin (Uličný, 2001).

Interpretations of the depositional history of the Turonian strata are presented using diagrams summarizing the T-R history of basin filling. The T-Rmax curves for intermediate to large-scale genetic sequences (Figs 2, 4; cf. Uličný et al., 2009) are derived from proximal - distal correlation panels such as in Fig. S1. Each regressive maximum is derived from the lateral position of the regressive limit of delta-front / upper-shoreface sandstones, correlated into the Bch-1 section and plotted at a corresponding depth, as a distance from Bch-1 site. In this regard, the T-Rmax curve is constructed as a ‘shore proximality through time’ diagram that can be applied in the similar way as a more typically used T-R curve, if limitations of the data are borne in mind, in particular the influences of changes in location of sediment input through time (Fig. 1).

Transgressive maxima are plotted in the Bch-1 log at depths of correlated maximum transgressive surfaces (MTSs), which, in all cases, have reached and stepped over the landward limits of the preserved basin fill. Variations in landward extent of transgressive

shorelines through time cannot be reconstructed for two reasons: (1) variations in coastal onlap cannot be reconstructed in the faulted graben infill without marginal terrestrial facies preserved; (2) within the graben fills, subaerial facies and subaerial slopes were reworked by subsequent transgressive ravinement (cf. Uličný et al., 2009). As a result, the transgressive shoreline distances are arbitrary and unified for all MTSs, based on estimated distance from the Bch-1 core to the inferred main entry points of clastics at the faulted basin margin: 75 km in the NW, and 130 km in the SE.

The SE depocentre is less completely preserved than that in the NW, with the most proximal part of the sub-basin eroded during the Late Cretaceous – Paleogene inversion of the Bohemian Massif (cf. Ziegler, 1990; Voigt et al., 2008b). The main flooding surfaces, except the base of TUR 2, are correlated from the NW to the SE depocentre. In ther SE, however, the equivalents to the composite genetic sequences defined in the NW are represented mainly by the downdip parts of prograding sandstone successions, mostly with significant amalgamation of the coarser clastic strata that prevents recognition of finer-scale sequences. For the construction of the T-R curve analogous to that of the NW depocentre, pinchout of fine-grained sandstones was chosen as the criterion for the regressive limit of sandstone bodies, due to paucity of preserved coarse-grained equivalents to delta-front or upper-shoreface strata.

While a single 2-D correlation panel, linking the two sub-basins, is presented in this paper (Fig. S1) to document the key proximal-distal stratigraphic relationships, plus the main biostratigraphic datum levels (Fig. 2), the spatial variability of individual sequences and interpreted shoreline trajectories is commented on below.

3.2.2. Cenomanian-Turonian boundary

The base of the Turonian is marked by an omission surface at 402.5 m, associated with a distinct hiatus (cf. Uličný et al., 1993; Čech et al., 2005). A second, less prominent, omission surface at 398.2 m, is overlain also by glauconite-rich, greenish-grey marlstone (Fig. 2). Calcareous nannofossil zones UC 5a-b (Burnett 1998), correlative to the upper part of the *M. geslinianum* and *N. juddii* ammonite zones, are absent, confirming the interpretation of Uličný et al. (1993) of a major hiatus at this time in the central part of the basin. The FO of *E. moratus* at 400 m depth indicates that at least nannofossil zones UC 5c – 6a are contained in the lowermost 2.35 m of the Turonian succession in Bch-1. Downlapping geometry of the basal TUR 1 strata is illustrated in Fig. S1 in the region c. 30-40 km west of Bch-1. The prominent earliest Turonian condensation event is attributed to the major flooding near the C-

T boundary that established hemipelagic conditions over most of the basin (cf. Klein et al., 1983, Uličný et al., 1997).

3.2.3. Early – early Middle Turonian

Upward from the base of the Turonian, the micritic marlstones of the Bílá Hora Formation, with locally abundant sponge spicules and an upward increase in silt content, correlate to sequences TUR 1-3 (Fig. 2). Because the initial locus of clastic deposition of TUR 1 and 2 was the most distant from the location of Bch-1 in the basin centre, equivalent intervals in the core are relatively condensed compared to the rest of the Bch-1 depositional record.

In the NW sub-basin, deltaic systems prograded both from the SW edge of the Western Sudetic Island (source NW I), and from a temporary source area of the Most-Teplice Palaeohigh of the Central European Island (source NW-III in Fig. 1). As a result, a major clastic wedge formed in the early Middle Turonian, prograding to the SE, obliquely along basin axis (Fig. 1; Uličný et al., 2009; Mitchell et al., 2010). This pattern persisted, with minor intervening transgressions, until the end of deposition of TUR 3.

In the SE sub-basin, a major prograding wedge containing a number of stacked, thin sandstone units, comprises strata equivalent to sequences TUR 1 and 2. The FO of *C. woollgari*, marking the base of the Middle Turonian, correlates to 374 m depth in Bch-1, and in both sub-basins appears some distance above the interpreted base of a lowstand systems tract (LST) of TUR 2.

The basal MTS of TUR 3 correlates to the glauconite- and phosphate-rich bed at 359.3 m, marking the base of the Jizera Formation (cf. Čech et al., 2011). It is correlated widely in the basin centre and into the SE, where this transgressive surface marks fast drowning of the entire depocentre. In the NW depocentre, the expression of this surface varies between a clear MTS in the western area, with a relatively lower long-term supply, and a rather subdued transgressive surface in the eastern part, where maximum supply was directed during the axial progradation of the TUR 2-3 deltaic system (cf. Uličný et al., 2009; Mitchell et al., 2010). The basin-scale correlations suggest that the highstand deposition of TUR 3 is condensed in the basal glauconitic / phosphatic bed in Bch-1, whereas most of the TUR 3 strata in the basin centre belong to a falling stage to lowstand systems tract (LST). The onset of the lowstand phase, characterized in the NW by long-term aggradation coeval with progradation, is correlated above the 340m depth in Bch-1.

Elemental and palynological proxies in TUR 2 and 3 in Bch-1 are difficult to explain directly in terms of the T-R history. The peak in Si/Al ratio under the base of TUR 3 is not

matched by an increased T:M ratio, whereas there is a marked increase in terrestrial palynomorphs above the basal MTS of TUR 3 (Fig. 2). An explanation is offered by the interplay of changing palaeogeography (due to both tectonics and sea-level change) and water circulation at that time. The increased Si/Al ratio in TUR 2 is interpreted as a signal of progradation of shorelines from the SE, aided by vigorous tidal currents toward the NW that dominated the seaway circulation at the time (cf. Mitchell et al., 2010).

Due to the vigorous water-mass circulation, marine palynomorphs dominated the T:M ratio until the end of TUR 2 deposition. The short-lived relative increase in terrestrial palynomorphs above the base of TUR 3 is correlated to a relative sea-level fall in the early part of deposition of TUR 3, enhanced by partial uplift in the western part of the basin (Uličný et al., 2009). This event led to closure, or significant narrowing, of the NW communication of the Bohemian Cretaceous seaway with NW Europe, which apparently resulted in a transient change of circulation pattern to one of a semi-enclosed embayment. Continued progradation of lowstand deltas from the NW is recorded in the interval of elevated T:M ratios above c. 350m depth, gradually decreasing towards the base of TUR 4 at 318m.

3.2.4. Late Middle to earliest Late Turonian

Deposition of TUR 4, towards the end of the Middle Turonian, was characterized by a series of vertically stacked, high-frequency sequences showing progradation of coarse-grained deltaic lobes in various directions depending on the accommodation available at different times. A tidal circulation regime was re-established (Uličný et al., 2009), with dominant role of SE-directed currents. TUR 4/1 is the thickest intermediate-scale sequence that prograded towards the Bch-1 site, and its youngest short-term sequence, pinches out at the shortest distance (26 km) from Bch-1. By contrast, deltaic wedges of TUR 4/3 prograded mainly to the SW (Uličný et al., 2009), and therefore in a SE-directed cross-section (Fig. S1) sequence TUR 4/3 appears as relatively backstepping to the NW.

The repeated regressive episodes within TUR 4 have no clear expression in the T:M and Si/Al ratios (Fig. 2), although the TUR 4 delta fronts from the NW reached closer to Bch-1 than older strata. This lack of response in parameters commonly used as proximality indicators shows that, in a current-swept seaway, a T-R history cannot be directly derived from variations in sediment composition or from T:M palynomorph ratios in basinal sites.

3.2.5. Late Turonian and the Turonian-Coniacian boundary

The transgressive event at the base of TUR 5 (246 m depth) is prominent basinwide and marks the onset of higher carbonate contents (Fig. S2) and more widespread cementation in

all facies, which culminate in TUR 6. The base of TUR 5 correlates to an acme of *Inoceramus perplexus* Whitfield, and is distinct in many cores due to abundant fragments of inoceramid prisms. This level is correlated to the "costellatus-plana Event" in NW Germany (Fig. 3). Composite sequences TUR 5 and TUR 6 comprise a number of short-term sequences but, at present, only a few intermediate-term sequences, superimposed on a long-term shallowing trend, can be traced with confidence to the Bch-1 core.

Sequence TUR 7 is confined mainly to a tectonically deepened marginal part of the NW sub-basin and sourced from both rejuvenated (Source I, Fig. 1) and newly emerging (Source II) local uplifts along the Lužice Fault Zone (Uličný et al., 2009). The base of TUR 7 is correlated tentatively to a zone of fine-grained mudstones above 130 m depth, and its top at an omission surface at 111 m with the *Didymotis* Event I located in core. In addition, three closely-spaced surfaces covered by glauconite- and sand-rich marlstones, occur between 116 and 119 m, and are correlated to internal, short-term transgressive surfaces within TUR 7.

Strata correlative to the CON 1 sequence are marked by decreased carbonate content (Fig. S2). The FO of *Cremnoceramus deformis erectus* (Meek), marking the base of the Coniacian, is correlated to 98 m depth (Figs 2, 3; Fig. S1). Further updip, this datum level occurs within the prograding clinoforms of a deep-water, Gilbert-type delta (Uličný et al., 2009). The marked increase in shore proximity in the T-R curve for CON 1 is caused by the emergence of a new uplift at the eastern end of the Western Sudetic Island, which shifted the source of clastics to a location close to Bch-1 (Source NW II, Fig. 1). The deltas prograded into water depths exceeding 80 to 110 m, before being eventually flooded during the early *Cremnoceramus crassus crassus* Zone (Fig. 2).

4. Carbon isotope record

4.1. Main features of the $\delta^{13}C_{org}$ curve

The Bch-1 core provides a high-resolution record of $\delta^{13}C_{org}$ values through the Turonian between 402.35 and 95 m depth (Figs 2, 3). The 50 cm sampling interval employed here represents 5.5 – 5.8 kyr. This permits comparison to the highest-resolution $\delta^{13}C$ curves available elsewhere (Fig. 3). The organic carbon-based curve shows values ranging between -27 and -25.2 ‰ (VPDB). In common with most other organic-matter-derived $\delta^{13}C$ curves, there is pronounced sample-to-sample variation in the data. To compensate for this, a curve smoothed by a 5-point moving average is used below for comparison with published $\delta^{13}C_{carb}$ curves and identification of the CIEs.

For the purpose of descriptive discrimination between relatively long- and short-term fluctuations within the Bch-1 record, a long-term $\delta^{13}C$ 'baseline' record is approximated by a 6^{th}-order polynomial curve (Fig. 2). Although arbitrary, the discrimination of short-term (< 10 m thickness) and intermediate-term (10 – 50 m) intervals of prevailing positive or negative values compared to the long-term baseline proves useful in discussing the possible relationships of the $\delta^{13}C_{org}$ fluctuations to the T-R record and the interpreted eustatic sea-level changes (see Discussion), and in comparing the potential time spans of different CIEs.

The baseline $\delta^{13}C_{org}$ trend shows broad maxima culminating near 160 and 340 m depths, a minimum near 240 m, and a decline of values towards the minimum at base of the Coniacian. Absolute maxima in $\delta^{13}C_{org}$ values occur at 140 m and near the 340 m long-term extreme.

4.2. Identification of CIEs: correlation to published curves

The smoothed $\delta^{13}C_{org}$ record shown in Fig. 3 shows close similarities to published $\delta^{13}C_{carb}$ curves (e.g. Jarvis et al., 2006) on long- and intermediate-term scales. Between stratigraphically neighbouring positive and negative CIEs, the difference in absolute $\delta^{13}C$ values is commonly larger in the smoothed $\delta^{13}C_{org}$ curve, by up to 0.5 – 0.7 ‰ (e.g. Hitch Wood-Navigation; Round Down – Glynde CIEs), than in correlative $\delta^{13}C_{carb}$ records (Fig. 3).

All 12 named CIEs in the Turonian (Jarvis et al., 2006) are identified in the Bch-1 record based on their defining criteria as inflection points of the long- to intermediate-term isotope profile, with biostratigraphic markers anchoring the correlations (Fig. 3; Supplementary Material). Several numbered, subordinate CIEs from Jarvis et al. (2006) have their counterparts interpreted in the Bch-1 record, as well as the 6 additional, numbered CIEs introduced by Voigt et al. (2007).

The comparison in Fig. 3 is deliberately focused on those $\delta^{13}C$ records accompanied by the highest available biostratigraphic resolution. Other published Turonian $\delta^{13}C$ curves, principally from the Tethyan realm, are typically derived from much thinner sections and pose problems with the compatibility of biostratigraphic schemes. These were not used for primary correlation, and the same applies to the wood-based record from Takashima et al. (2010). The salient features of the $\delta^{13}C$ record in Bch-1, however, are correlatable, albeit with lower resolution, also to the Tethyan sections (Galeotti, 2006; Jarvis et al., 2006; Wendler et al., 2011, Sprovieri et al. 2013).

In the lowermost part of the Bch-1 section, the major positive excursion of the OAE2 CIE is absent due to the hiatus described above. This omission is in contrast to the marginal part of

the basin where most of the OAE2 CIE is preserved (Uličný et al., 1997). Correlations in Fig. 3 indicate that the condensed section above 402.35 m contains much of the earliest Turonian *Watinoceras devonense* Zone.

In the Lower to Middle Turonian, the most prominent positive CIEs represent inflection points that are culminations of intermediate-term positive fluctuations relative to the long-term baseline: Tu3, Round Down or the 'Pewsey' CIEs. Other $\delta^{13}C$ peaks, such as Tu1/Holywell or the 'g1' CIE, are represented typically by less than 5 m thick intervals (Fig. 3). Even considering generally reduced depositional rates compared to the rest of the section below 370 m depth, these thin intervals of $\delta^{13}C$ fluctuations are viewed as short-term departures from intermediate-term trends.

Contrasting relationships can be found when comparing the intermediate- vs. short-term trends, in many cases of both positive and negative CIEs (Fig. 3). Whereas the Lulworth negative CIE is placed at the extreme of an intermediate-term minimum within a long-term *rising* $\delta^{13}C$ trend near 375 m, another prominent negative CIE, the Glynde Event, seems confined to a 10 m-thick interval of sharply lowered values during a long-term *fall* in $\delta^{13}C$. The 'Pewsey' CIE is followed by a region of prevailing low $\delta^{13}C$ values that correspond to the Middle to Upper Turonian 'plateau' recognized by Jarvis et al. (2006). In the 'plateau' region, the Lower and Upper Southerham and Caburn CIEs are fairly short-term fluctuations also in the Chalk, but their correlation with Bch-1 is aided by the well-defined FO of *I. perplexus* in the Bohemian Cretaceous, correlated to the FO of *Subprionocyclus neptuni* (Geinitz) in the Chalk, and marking the base of the Upper Turonian. At 228 m, the Bridgewick CIE is interpreted in the inflection point from falling to rising intermediate-term trends.

The greatest difference from the reference isotope profile of the Chalk is present in the Upper Turonian, where the higher resolution of the Bch-1 data shows a significantly more complicated intermediate- and short-term pattern in the region of the Hitch Wood CIE (Fig. 3). Based on the correlations presented here, additional peaks are defined as part of a Hitch Wood Event 'suite'. The Hitch Wood 1 (HW1) CIE is defined at the intermediate-term peak within a long-term rising trend at the level of the *Hyphantoceras* Event (cf. Wiese et al., 2004; Jarvis et al., 2006). Newly defined HW2 and HW3 are closely-spaced peaks (HW2 coinciding with the long-term maximum near 135 m), separated by a sharp short-term trough. This detailed structure of the $\delta^{13}C$ trends seems to be amalgamated into a single inflection from

rising to falling values in the Chalk data, interpreted here as due to significant condensation at several regional hardground surfaces (cf. Gale, 1996; Jarvis et al., 2006).

A markedly similar combination of long- and intermediate-term trends as in Bch-1 is found in the Liencres section, northern Spain (Fig. 3). Based on the position of '*Didymotis* 0' faunal event in Liencres, HW 3 in Bch-1 should correspond to the 'Peak +2' CIE of Wiese (1999). In the classical North German section of Salzgitter-Salder, however, a long-term decrease is values occurs above the HW1 Event, with subdued amplitudes of shorter-term fluctuations. The correlation of the '*Didymotis* 0' biostratigraphic marker suggests that levels equivalent to the HW2 and 3 are most probably present in Salder, but with more subtle amplitudes of $\delta^{13}C$ anomalies. A more precise correlation of the HW CIE suite from Bch-1 to Liencres and Salzgitter would benefit from revision of the FOs of *P. germari* and *M. scupini* in the outcrop sections. The Navigation negative CIE, coinciding to the correlated FO of *C. deformis erectus* (cf. Walaszczyk et al., 2010), is a well-defined extreme of the intermediate-term minimum from 85 to 110 m depths, superimposed on a falling long-term trend across the Turonian-Coniacian boundary. The interval from the HW 3 CIE to the Navigation CIE in Bch-1 indicates relative condensation compared to time equivalents in Liencres and Salzgitter (Fig. 3).

4.3. Comparison between organic-based and carbonate $\delta^{13}C$ records

The comparison of the $\delta^{13}C_{org}$ record in Bch-1 against carbonate-based records (Fig. 3) shows a close similarity of relative trends in $\delta^{13}C$ between the organic- and carbonate-based datasets, in agreement with previous observations of links between the carbonate and organic C reservoirs (Arthur et al., 1988; Hayes et al., 1989). Differences in amplitude between $\delta^{13}C_{carb}$ and $\delta^{13}C_{org}$ in coeval parts of CI curves, or lags in excursions in $\delta^{13}C_{org}$ compared to $\delta^{13}C_{carb}$ can occur, mainly due to variations in pCO_2 and isotopic composition of atmospheric CO_2 (Popp et al., 1988; Gröcke et al., 1999; Kump & Arthur, 1999; Jarvis et al., 2011).

In Fig. 3, differences between the amplitudes of short- to long-term trends in the smoothed record $\delta^{13}C_{org}$ of Bch-1 and the $\delta^{13}C_{carb}$ records are smaller than expected. For instance, between the Round Down and Bridgewick CIEs, the long-term shift is 1.5 per mil in $\delta^{13}C_{carb}$ (English Chalk) and 1.7 per mil in $\delta^{13}C_{org}$ (Bch-1). In some cases, short- or intermediate-term fluctuations are even larger in some carbonate records: in the Lower Turonian, larger discrepancies exist in $\delta^{13}C$ amplitudes between the Chalk and Oerlinghausen curves (both

carbonate-based) than between Oerlinghausen and the $\delta^{13}C_{org}$ of Bch-1. These differences likely result from varying diagenetic overprints in the $\delta^{13}C_{carb}$ data.

Evaluation of T:M ratios, used as a proxy for terrestrial vs. marine OM ratios, shows no systematic relationship with the $\delta^{13}C_{org}$ (Fig. 2). Distribution of n-alkanes suggests a very consistent source of aquatic OM throughout the succession, without evidence for significant terrestrial OM contribution (Supplementary Table ST3). In general, the biostratigraphically controlled correlations in Fig. 3 indicate that the smoothed $\delta^{13}C_{org}$ record in Bch-1 overwhelmingly reflects a global reservoir signal.

Main differences between the curves compared in Fig. 3 clearly result from differences in sedimentation rate histories and presence of hiati, such as at the C-T boundary and condensed lowest Lower Turonian in the Bch-1 record, or expanded Upper Turonian Hitch Wood CIE suite. The coeval interval in the Liencres curve (Fig. 3), although carbonate-based, shows pronounced fluctuations similar to $\delta^{13}C_{org}$ in Bch-1. This fact probably prevents a theoretical interpretation of a change in $\Delta^{13}C$ linked to changing pCO_2 at that time (cf. Kump & Arthur, 1999; Jarvis et al., 2011), which might be employed to explain smaller amplitude short-term variations in $\delta^{13}C_{carb}$ in Salzgitter,

Similar single-peak expression of the Hitch Wood CIE as in the condensed Chalk record is found in Tethyan sections (cf. Jarvis et al., 2006), but due to uncertain macrofossil biostratigraphic correlation to the Tethyan realm, it is not clear whether these peaks correspond to the *Hyphantoceras* Event, as the Hitch Wood 1 CIE does in NW Europe, or perhaps to some of the higher peaks in the *M. scupini* Zone shown in Bch-1 (Fig. 3). In the original correlation chart of Wiese (1999 fig. 4), marked condensation and/or a hiatus is shown in the Salzgitter-Salder section at the level equivalent to the Hitch Wood 2 peak at Liencres (between 100 and 120 m, cf. Wiese 1999 fig. 1), and Richardt & Wilmsen (2012) interpreted an unconformity (their SB Tu 5) near this level at Salzgitter.

5. Discussion

5.1. Eustatic signatures interpreted from T-R history

For the following discussion of potential climate-driven, short-term sea-level changes, and their relationship to variations in $\delta^{13}C$, it is critical to assess to what extent a eustatic signature can be derived from the Bohemian Cretaceous Basin fill and which part of the T-R history of each sub-basin was controlled by local factors. In the case of incompletely preserved basin

fills, such as the infills of graben sub-basins of the Bohemian Cretaceous Basin, not even a picture of *relative* sea-level (RSL) change can be fully, quantitatively established from an evaluation of the sub-basin fill alone. Clearly, an attempt to invert each of the T-R records from the two sub-basins (Fig. 2) directly into a RSL history, assuming constant sediment supply and subsidence rates, would result in two different RSL interpretations.

The analysis of changes in stratal geometries in the NW sub-basin by Uličný et al. (2009b) showed how the fluctuations in tectonic subsidence rate in the depocentre, temporal and spatial variations in clastic supply, and localized temporary uplifts contributed to the T-R history of the deltaic systems. Because of these intrabasinal influences, the large-scale genetic sequences TUR 1 – CON 1 in the Bohemian Cretaceous Basin differ strongly in their duration. Genetic sequences are localized sedimentary bodies and they can not be taken as representing eight depositional cycles of equal hierarchical rank. At the current stage of knowledge, the focus is on qualitative derivation of events in basin-fill history that are best explained in terms of extrabasinal base-level change.

In Fig. 2, the T-Rmax records from the two sub-basins are compared and a tentative sea-level curve is shown, based on a set of criteria more extensively discussed by Uličný et al. (2009), and only briefly reviewed here. Theoretically, any temporary acceleration in subsidence can cause a transgression, and therefore only those maximum transgressive surfaces that correlate between the two sub-basins are evaluated as potentially eustatically driven, and, where possible, verified by data from other basins. In a subsiding basin, it is the evidence for basin-scale base-level *falls* counteracting subsidence (i.e. not driven by temporary uplift) that can be evaluated with greater confidence as reflecting eustasy. Offlapping stratal geometries, long progradation distances, and downdip coarsening of grain size are used to interpret regressions forced by base-level falls (cf. Posamentier & Allen, 1999), and to infer extra-basinal (mainly eustatic) controls on base level.

Response times of the Bohemian fluvio-deltaic systems to allogenic forcing such as a base-level fall were probably short, on a scale of several kyr, due to the limited sizes of drainage basins and resulting time-averaged sediment supply (cf. Swenson & Muto, 2007). Therefore, time lags between the base-level change and T-R shoreline response are not expected to be significant in case of short-term sequences of 100 – 500 kyr duration.

Points of maximum sea-level fall, terminating the falling stage systems tracts, and marking the onset of lowstand deposition, are assumed to slightly pre-date the terminal regressions that mark the end of lowstand deposition and the turnaround towards transgression. In most short-

term sequences, however, the stratigraphic resolution does not allow the falling stage and lowstand deposits to be distinguished (Uličný et al., 2009).

The tentative sea-level curve in Fig. 4 shows short-term sea-level lows where forced regressions are interpreted in the NW sub-basin, or simultaneously in both sub-basins. The chronostratigraphic dating of interpreted sea-level falls is constrained by the Bch-1 $\delta^{13}C$ data and biostratigraphy and awaits future verification from comparable datasets elsewhere. Estimates of magnitudes of individual sea-level cycles are necessarily speculative, in the order of 10 m in most cases. Superimposed intermediate to long-term trends (deepening / shallowing) are interpreted from successions of short-term fluctuations in which relative elevations of successive sea level minima are based on the relative positions of maximum regressive shorelines, after intrabasinal factors such as initial palaeodepth, increased supply, or uplift are considered. Higher long-term subsidence rate through time required larger magnitudes of short-term sea-level falls to cause forced regressions. A more quantitative derivation of a range of possible sea-level scenarios requires a numerical modelling approach and is beyond the scope of this study.

In the text below, long- versus intermediate to short-term signals interpreted in the basin fill are discussed separately, in order to aid comparison to published estimates of sea-level changes that vary in temporal resolution. This separate discussion, however, does not imply an assumed separation of potential causal processes.

5.1.1. Long-term signal

On a long time scale (1-2 Myr), Uličný et al. (2009) found agreement between the main features of the T-R history of the NW sub-basin (although increasingly affected by local tectonics in Bohemia during the Late Turonian – Coniacian) and various published estimates of eustatic change. A long-term trend interpreted here from T-R data from both sub-basins and Bch-1, as shown in Fig. 4, broadly agrees with: (1) the globally recognized earliest Turonian flooding (base TUR 1 with condensed section); (2) a mid-Turonian long-term low, culminating in TUR 4; (3) a terminal Turonian though early Coniacian sea-level rise culminating during the *C. crassus crassus* inoceramid zone on top of CON 1 sequence (cf. Gale, 1996; Galeotti, 2006). In the New Jersey coastal plain the Late Turonian – early Coniacian record is affected by chronostratigraphic uncertainty, but in the Western Interior Seaway an early Coniacian transgression is a part of the peak long-term flooding of the Niobrara Cycle (Kauffman & Caldwell, 1993). A general similarity is found between the long- term sea-level trends in Gale (1996) and the inferred long-term sea level trend from the

Bohemian Cretaceous Basin (Fig. 4). The resolution of sequence stratigraphy in Gale (1996) does not permit interpretation on time scales less than 1 Myr, and hiatuses in the Upper Turonian part of the Gale (1996) curve make the comparison uncertain in that interval. The specific setting of the Chalk sea may have been favourable for recording long-term eustatic trends, perhaps more closely than clastic basins in which a base-level signal is filtered through dynamics of fluvio-deltaic systems. It has to be noted, however, that the above similarities still carry a great deal of uncertainty due to differences in biostratigraphic detail, for instance, in case of the latest Turonian sea-level rise (compare Gale, 1996 vs. Voigt & Wiese, 2000).

5.1.2. Intermediate- to short-term signal (<500 kyr)

A number of short-period, long-distance regressions occur within sequences TUR 2 – 6 that were likely forced by relative sea-level falls. Within TUR 2 sequence, a forced regression interpreted from offlapping geometries in the NW sub-basin by Uličný et al. (2009) is coeval to the longest-distance regression in the SE, at the end of the early Turonian (prior to Lulworth CIE). This level correlates to an intermediate-term sea-level low of Gale (1996) (Fig. 4), as well as to an unconformity in the Münsterland Basin (SB Tu1 in Richardt & Wilmsen, 2012). In both sub-basins the TUR 2 maximum regression distance was probably enhanced by previous filling of the depocentres during TUR 1 regressive episodes.

A forced regression is clearly documented during early phase of TUR 3 deposition in the NW, but the involvement of partial tectonic uplift and increased clastic supply was probably substantial. The marked progradation of TUR 3 in the NW, contrasting with the lack of coeval regressive wedges in the SE, was enhanced by previous filling of accommodation space by earlier deltaic wedges. Several episodes of minor SL fluctuations are suggested by changing ratios between progradational and aggradational component in the NW. In the SE, proximal strata of TUR 3 did not reach the area of preserved basin fill and hence a base-level history cannot be derived except the deepening inferred from facies changes correlative to c. 340-345m depth in Bch-1. This level correlates to the Round Down CIE interpreted by Jarvis et al. (2006) as coeval with a major flooding episode in the early Middle Turonian.

TUR 4 sequence contains a cluster of prominent regressive wedges in the late Middle Turonian, with several MTSs correlative between the NW and SE sub-basins despite varying data resolution. Uličný et al. (2009) interpreted short-term eustatic falls as the cause of forced regressions in TUR 4, marked by long-distance (>50 km) progradation of several very coarse-grained deltaic units across the main subsiding depocentre in the NW sub-basin, at a time of moderately increasing long-term subsidence rates compared to previous sequences.

The basal maximum transgression of TUR 5, pre-dating the Caburn CIE, is the most prominent Turonian correlation level in the entire basin and correlates to an early Late Turonian transgression in other basins, coinciding with the *I. perplexus* Event (e.g. Richardt & Wilmsen, 2012).

TUR 5 in general is dominated by an intermediate-term regression, with a number of high-frequency transgressive episodes superimposed, similar to TUR 6. The apparent increase in frequency of RSL changes in the Late Turonian appears similar to interpretations of regional RSL histories by Gardner (1995) and Sahagian et al. (1996), but correlation of individual events is not possible. Further work is necessary to elucidate the details of Late Turonian depositional history in the Bohemian Cretaceous Basin. This applies also to the TUR 7 sequence that was partly affected by accelerated subsidence (Laurin & Uličný, 2004; Uličný et al., 2009). Whereas in the NW increased clastic supply compensated for the rapid deepening, in the SE the supply rate either did not change or decreased and the time of TUR 7-CON 1 is marked by a condensed succession. A minor short-term sea-level drop in TUR 7, suggested by Uličný et al. (2009) for the NW sub-basin, may be supported by the interpretation of an unconformity within the *M. scupini* Zone by Richardt & Wilmsen (2012), but would remain undetected in the SE.

A terminal Turonian short-term regression, superimposed on a long-term sea-level rise, is interpreted to fall within sequence CON 1, as defined by Uličný et al. (2009), close to the Turonian-Coniacian boundary. A shallowing episode at this level is consistent with development of hardgrounds in many parts of Europe (Olszewska-Nejbert, 2004; Jarvis et al., 2006), and with evidence of a latest Turonian unconformity and lowstand in the North American Western Interior (Shank & Plint, in press; Walaszcyk et al., in revision).

Time intervals represented by individual short-term sequences in Bch-1 can be estimated relatively easily in the Middle Turonian, which offers the best resolution of physical correlations. The interval between 246 and 328 m depth correlates to 8 most prominent, short-term, composite sequences within TUR 4 and the uppermost part of TUR 3. Using the average sedimentation rate of 9 cm/kyr, this interval is estimated to be approximately 911 kyr, with individual progradation episodes representing, on average, less than 114 kyr. This estimate is admittedly crude and the number of sequences is a minimum value due to difficulties in correlating some bounding surfaces from the SW part of the sub-basin.

With the long-term subsidence rate at that time near 90 m/Myr, the rate of eustatic drop required to overcome the subsidence rate falls within the range of rates attributable only to glacial eustasy (Dewey & Pitman, 1998; Miller et al., 2005, 2011). Autogenic mechanisms

such as lobe shifting were clearly involved in the formation of elementary sequences (cf. Uličný et al., 2009) that occurred on yet shorter time scales and are not correlatable basinwide.

A similar timing of interpreted short-term forced regressions (100 kyr and shorter), with amplitudes near 10 m, has been reported in detailed studies of the Middle Turonian of Western Canada (Varban & Plint 2008) and Utah (Zhu et al. , 2012). High-frequency base-level changes, probably driven by eustasy, were previously interpreted by Gardner (1995) in the Western Interior Seaway, but confident correlation was prevented by uncertainties in biostratigraphy. Significant error bars of bentonite ages, and a lack of biostratigraphic data in Zhu et al. (2012) also pose a correlation problem. Sea-level changes interpreted in the Turonian to early Coniacian by Sahagian et al. (1996) from the Ust-Yenisey Basin of northern Siberia, cannot be used for direct comparison because of uncertainties in biostratigraphy which, in addition, was "enhanced" by using the Haq et al. (1988) 'global' sea-level curves as a template (see Sahagian et al., 1994 for details on data handling).

A special case is the eustatic event interpreted by Bornemann et al. (2008) at the level of the 'Pewsey' CIE, based on a local peak in planktonic foraminifera $\delta^{18}O$. However, the biostratigraphic (nannofossil) data are not entirely consistent with carbon-isotope-based correlation presented in the same paper (Bornemann et al., 2008, their Fig. S2), because the interpreted 'Pewsey' CIE at ODP Site 1259 is correlated to the (much older) base of the CC12 Zone, and the inferred base of the Coniacian is problematic with respect to both the Navigation negative CIE and the likely diachronous FO of *Marthasterites furcatus* (Deflandre in Deflandre & Fert, 1954), the uppermost Turonian CC13 zonal index species (Lees, 2008). It is suggested here that both the interpretation of the CI stratigraphy and the biostratigraphy for this part of Site 1259 should be re-evaluated, and that the $\delta^{18}O$ peak in Bornemann et al. (2008) may correlate to an older level than the 'Pewsey' CIE.

Takashima et al. (2010) interpreted a short-term shallowing event (their SS1 unit) to coincide with the 'Pewsey' CIE. If their carbon isotope correlation is correct (Takashima et al., 2010 figs 6, 7, 9), SS1 correlates to an interval spanning at least the Round Down through 'Pewsey' CIEs, i.e. almost 1 Myr, equivalent to most of TUR 4 and uppermost TUR 3 sequences (Fig. 4). This entire interval is shown here as dominated by lowered long-term sea level, with numerous short-term fluctuations superimposed, so while the SS 1 unit in the Yezo Group could be an expression of long-term shallowing, it is impossible to associate the Pewsey CIE with a single short-term sea-level event, or limit the mid-Turonian shallowing solely to the time of this CIE.

5.1.3. Time scales of Cretaceous sea-level change and stratigraphic resolution

Along with problems with stratigraphic resolution noted above, the issue of different time scales considered for Cretaceous sea-level changes is encountered if one attempts to test, via inter-regional correlation, any of the claims either in favour of, or against, potential glacially driven sea-level falls. Modelling by Flögel (2011) suggests that potential glacial episodes, under some scenarios of orbital parameters and pCO_2, would have occurred (and waned) on a time scale as short as 20 kyr, and mostly within the 100 kyr short eccentricity band. This theoretical prediction is in contrast with the low-resolution of bio- and chemostratigraphy in many studies that so far have suggested evidence for glacioeustatic falls (Miller et al., 2005; Galeotti et al., 2006; Bornemann et al., 2008; Browning et al., 2008).

In Fig. 4, the extent of the mid-Turonian peri-platform lowstand (and corresponding hiatus in platform strata) from Galeotti et al. (2006) is plotted according to their correlation of the Lazio-Abruzzi $\delta^{13}C_{carb}$ curve to the Contessa and Chalk records (their figs 1 and 9), as ranging from the Glynde to below the Hitch Wood 1 CIEs, i.e. extending for at least 1.2 Myr. However, according to foraminifera biostratigraphy, Galeotti et al. (2006) date the beginning of this lowstand as the middle Early Turonian, closer to the age of strata below 'the' middle Turonian hiatus in New Jersey (cf. Sugarman et al., 1999). Further work is needed either to clarify the biostratigraphic calibration, or to re-evaluate the CI data from the Lazio-Abruzzi section, or both.

Comparison of the relatively low-resolution New Jersey and Lazio-Abruzzi data with the T-R record developed here (Fig. 4), underlines the importance of high stratigraphic resolution in interpreting sea-level histories. It is proposed here that the multiple sea-level fall events of approximately 10 metres magnitude on 100 kyr or shorter time scales that are particularly conspicuous during parts of the Middle Turonian, may represent records of individual cooling events, whereas the prominent unconformities in low-accommodation settings such as the New Jersey margin, Tethyan platforms or the interior of the Russian platform (Sahagian et al., 1996), most likely represent amalgamated, long-term records of a multitude of much shorter-lived events.

The differences in dating of the presumed 'main' mid-Turonian lowstand between Haq et al. (1988), Sahagian et al. (1996), Stoll & Schrag (2000), Miller et al. (2003) and Galeotti (2006) are partly a result of problems with stratigraphic resolution and interpretation. Some real discrepancies between basins in the timing of significant unconformities, however, are likely to be caused by different timing of RSL extremes and sedimentation rate variations, due to different tectonic regimes and the inevitable differences in individual basins' response

times to allogenic forcing. For these reasons, the use of prominent unconformities such as those in New Jersey to define '3rd-order' sequences and link them to the 2.4 Myr long eccentricity cycle (cf. Boulila et al., 2011) seems premature. Considering the small magnitudes of sea-level fall, typically under 40 m, the 2.4 Myr period is far too long to be the principal cycle generating unconformities in tectonically active basins, where rate of eustatic fall must exceed the subsidence rate. Further understanding of the hierarchy and causes of Cretaceous sea-level changes should build primarily on high-resolution records of the most complete sections, linked by very high-resolution $\delta^{13}C$ and biostratigraphic data.

5.2. $\delta^{13}C$ and sea level – a causal relationship?

The concept of a causal link between sea-level change governing carbon burial, and resulting fluctuations in $\delta^{13}C$ (Scholle & Arthur, 1980; Mitchell et al., 1996; Jarvis et al., 2002) originally considered long-term (stage / substage resolution) sea-level changes. This was largely because the typical resolution of $\delta^{13}C$ datasets in 1980s – 90s was much lower than today, and perhaps also because shorter-period eustatic change in the mid-Cretaceous greenhouse was not considered possible. The recognition of a fine-scale structure of CIEs correlatable on a time scale of 100 kyr (Jarvis et al., 2006, Voigt et al., 2007), as well as the growing evidence for sea-level changes on similarly short time scales, indicate that the picture is much more complex, and underlines the importance of the temporal resolution at which observations are made and the process-response ties that are inferred. Therefore, the comparison between $\delta^{13}C$ and interpreted sea-level records, below, is first discussed separately for long-term and intermediate- to short-term $\delta^{13}C$ fluctuations.

5.2.1 Long-term signal

The long-term baseline derived from the $\delta^{13}C_{org}$ record shows a markedly cyclic shape, with long-term maxima near the Round Down and Hitch Wood 2 CIEs, and a long-term minimum, approximately from the Glynde CIE to the 'h1' peak above the Bridgewick CIE (Figs 2, 3). In both sub-basins of the Bohemian Cretaceous Basin, the 'plateau' and the preceding falling limb of the long-term record coincide with an interval dominated by successive long-distance progradation episodes within TUR 4 and TUR 5, with a number of subordinate flooding events and a single major intermediate-term flooding event at the base of the TUR 5 sequence. Both long-term maxima show more prominent transgressive events than the long-term low, although they contain marked short-term regressions as well. The

interpreted long-term Chalk sea-level curve (Gale, 1996), adjusted to the Bch-1 isotope stratigraphy in Fig. 4, appears roughly in phase with the $\delta^{13}C$ long-term baseline. The long-term low in the $\delta^{13}C_{org}$ baseline correlates roughly to the shorter estimate of duration of the mid-Turonian hiatus on the Apulian platform (i.e. with its onset plotted according to the C-isotope correlation of Galeotti et al., 2006).

5.2.2. Intermediate- to short-term $\delta^{13}C$ fluctuations and sea level

The improved resolution of $\delta^{13}C$ datasets available since the 1990s has increased the likelihood of finding short-term, globally correlatable fluctuations. On the other hand, in many cases the high-resolution $\delta^{13}C$ curves indicate a more complex structure for some previously defined excursions (e.g. the 'Pewsey' or Hitch Wood CIEs, Figs 3, 4). Overall, many short- to intermediate-term $\delta^{13}C_{org}$ fluctuations in Bch-1, spread over 10 – 30 m thickness, contain several short-term T-R events of similar expression in the basin fill, in some cases causing problems in correlating a particular $\delta^{13}C$ fluctuation to a single event (Fig. 4). In Fig. 4, arrows next to the $\delta^{13}C$ curve show short-term sea-level fluctuations, both positive and negative, interpreted to occur near, or correlate directly to (black arrows), prominent CIEs.

Only in two cases the maximum transgressive surface bounding the Bohemian genetic sequences coincide with positive $\delta^{13}C$ anomalies: the base of TUR 3 correlates to an interpreted equivalent of Tu 7 CIE (Voigt et al., 2007), and base of TUR 6 to the h3 peak of Jarvis et al. (2006). The base of TUR 1 sequence coincides with a condensed record of several short-term anomalies and in case of TUR 7 the interpreted sea level rise seems equally close to either a positive or a negative short-term CIE. On the contrary, the prominent sea-level rise at the base of TUR 5 is not matched by any marked positive or negative $\delta^{13}C$ fluctuation. The Round Down CIE, one of the most prominent peaks in the Bch-1 data, correlates to the pulse of sea-level rise interpreted at 340-345m depth in Bch-1 but less prominent than the base of TUR 3. compensated by effects of tectonically forced sediment supply exceeding accommodation. Within sequence TUR 4, $\delta^{13}C$ maximum of the 'Pewsey' CIE does coincide with a short-term transgression, but, at the same time, two episodes of sea-level fall correlate immediately above and below this level, within the broad region of elevated $\delta^{13}C$ values that can be considered the 'Pewsey' CIE *sensu lato*.

Among the negative CIEs listed in Jarvis et al. (2006), the Lulworth $\delta^{13}C$ troughs coincides in the Bohemian Cretaceous Basin with a major regression and probably the negative extreme

occurs very close to the end of the interpreted sea-level fall and onset of lowstand progradation. The trough of the Glynde CIE occurs closer to a sea-level rise event than to a preceding fall, which coincided to a short-term $\delta^{13}C$ peak. The Bridgewick negative CIE, correlated to a major regression by Jarvis et al. (2006), occurs within an intermediate-term regression of TUR 5, but the narrow CIE interval correlates to an indistinct short-term regressive event at the limit of correlation resolution. The Navigation CIE correlates to the bottom part of the regressive wedge of the CON 1 sequence, but the extreme negative values actually post-date a short-term transgression (fig. 4)

If phase relationships between short-term sea-level and isotope events are ambiguous, intermediate-term intervals (c.30-50m thickness in Bch-1) might theoretically be considered less prone to correlation error and "noise" in the $\delta^{13}C$ record. A comparison of the intermediate-term sea-level trend derived from smoothing the short-term cycles (Fig. 4, grey line) brings equally ambiguous results, however. While crude in-phase coincidences can be seen in parts of the Lower and early Late Turonian, the Late Turonian intermediate sea-level trends appear out of phase with $\delta^{13}C$ in TUR 6. Notably, the terminal Turonian sea-level rise beginning near 140 m depth in Bch-1, with maximum depths in the basin attained roughly between the time of the *Didymotis* I Event and the T-C boundary, correlates to a steady decline in $\delta^{13}C$ values from the Hitch Wood 2 CIE upwards.

Clearly, despite individual matches described above, neither a systematic in-phase, nor out-of-phase correlation with interpreted sea-level cycles can be demonstrated at the level of short-term and intermediate $\delta^{13}C$ fluctuations (Fig. 4). The current stratigraphic resolution does not permit a correlation between phases of sea-level change driving the short-term T-R fluctuations and $\delta^{13}C$.

5.2.3. Time scales and potential orbital links of Turonian $\delta^{13}C$ fluctuations

A broad correlation exists between the Turonian $\delta^{13}C$ record and the inferred sea-level history at the level of general long-term trends and, partly on the intermediate time scale. A causal link employing long-term sea-level changes driving long-term $\delta^{13}C$ is not proven, however, because the long-term trends, based on the Bohemian Cretaceous genetic stratigraphy, are seen rather as intervals of *prevailing* short-term shallowing vs. deepening conditions (Fig. 4). Interpreted relative sea-level falls, as well as prominent transgressions correlated across regions, suggest the principal role of short-term (eccentricity-scale and shorter) sea-level changes that in several cases do show correlation to apparent in-phase

fluctuations in $\delta^{13}C$, but commonly are out-of-phase or have equivocal relationships, due to uncertainties of intra-basinal correlation.

The lack of decisive support for a phase link between sea level and $\delta^{13}C$ on short time scales need not be taken as a dismissal of potential causal relationship. Jarvis et al. (2002), for example, presented evidence for an in-phase relationship in the Campanian, at the level of < 750 kyr. The question is whether the in-phase relationships, documented in some intervals of geological time, point to an intermittently emerging causal link on some longer time scales, or rather to a parallel response of sea level and the carbon cycle to external climatic forcing. The latter appears likely if the potential orbital time-scales of short-term glaciations are considered (cf. Flögel et al., 2011).

Individual $\delta^{13}C$ excursions on short or intermediate time scales should not be immediately associated with individual sea-level events, or the shapes of $\delta^{13}C$ curves used to directly infer systems tracts in sedimentary sequences. Even if long-term trends in eustatic sea level are eventually proven to coincide with $\delta^{13}C$ variation, they are likely to have different expressions in basin fills due to accommodation and supply variations that define the systems tracts as spatially localized sedimentary bodies. From the practical point of view, however, this does not compromise the use of the network of defined CIEs for high-resolution correlation purposes.

The conceptual link between organic matter burial and exhumation, related to rising and falling sea level, respectively, remains a potential mechanism that needs to be explored by quantitative models as one of many interacting process links in the carbon cycle. Modelling of Cretaceous carbon cycle has not yet addressed potential effects of short-term perturbations and their superimposition on longer-term trends, with regard to time lags and/or cumulative effects in $\delta^{13}C$ on longer time scales. Bjerrum et al. (2006) focused on responses of the carbon cycle to a single sea-level rise, of < 40 m magnitude, lasting 100 – 400 kyr. Kump & Arthur (1999) explored the sensitivity of carbon cycle to perturbations lasting 500 kyr, much longer that the presumed 100 kyr residence time of carbon.

The time span between the peaks of the baseline cycle, or the absolute $\delta^{13}C$ maxima at the Round Down and Hitch Wood 2 CIEs, is between 2.2 and 2.3 Myr (based on average sedimentation rate for the Middle to Late Turonian of 9 cm/kyr). Given the uncertainty in radiometric dating (Ogg & Hinnov, 2012) and age interpolation in the Bch-1 core, it is plausible to consider a link to the 2.4 Myr eccentricity cycle. Intermediate-scale $\delta^{13}C$ fluctuations in the Lower to low Middle Turonian were interpreted by Voigt et al. (2007) as

corresponding to the 400 kyr eccentricity cycle, without direct inferences on relationships to sea level. A potential relationship between those peaks and T-R events in Bch-1 cannot be addressed at the current data resolution.

Cramer et al. (2003), analyzing Palaeocene $\delta^{13}C$ data, suggested that the long residence time of carbon in the oceans amplifies the response of the $\delta^{13}C$ records to longer forcing periods, and a similar conclusion was reached by Pälike et al. (2006) on Oligocene material. With the 400-kyr signal interpreted in Cretaceous $\delta^{13}C$ records (Voigt et al., 2007; Giorgioni et al., 2011), the possibility of expression of the 2.4 Myr eccentricity signal in the Cretaceous carbon cycle and, potentially, even longer time-scale modulation (Boulila et al., 2012; Sprovieri et al., 2013) should be considered, and the critical role of varying carbon residence times further explored.

6. Conclusions

Short-term transgressive-regressive fluctuations demonstrated in the Turonian of Bohemia bring further support for the existence of short-term, eustatic changes potentially driven by transient glacial events during the mid-Cretaceous greenhouse climate. Previously reported episodes of sea-level falls in low-accommodations settings such as the New Jersey margin or the Apulian platform, of 1 – 2 Myr duration, are proposed to represent amalgamated records of repeated sea-level fluctuations on 100 kyr scale, that are not recognizable in low-resolution datasets.

Considering the small magnitudes of sea-level falls, typically under 40 m, the 2.4 Myr period suggested by some to generate 3rd-order cycles, is far too long to be the principal cycle generating unconformities in tectonically active basins where rate of eustatic fall must exceed the subsidence rate. The correlation of intermediate- to short-term transgressive-regressive events in the Bohemian Cretaceous Basin to a high-resolution $\delta^{13}C_{org}$ curve makes it possible, in the near future, to compare the Bohemian record to datasets of similar, or yet higher resolution both in $\delta^{13}C$ and physical stratigraphy, in order to accomplish confident correlation on 100 – 400 kyr eccentricity time scales, and assess the timing of sea-level changes.

The key role of stratigraphic resolution applies also to the disputed relationship between sea-level and $\delta^{13}C$ records. A long-term "background" $\delta^{13}C$ cycle shows a duration close to the 2.4 Myr long-eccentricity cycle, and the long-term (1 Myr scale) highs and lows in $\delta^{13}C$ appear to roughly correspond to intervals characterized by more pronounced short-term sea-level highs and lows, respectively. On the scale of intermediate to short-term $\delta^{13}C$

fluctuations, a systematic relationship between $\delta^{13}C$ and interpreted sea-level change is not found. Clearly, however, on time scales below 1 Myr, it is not possible, even at this relatively high stratigraphic resolution, to associate individual fluctuations in $\delta^{13}C$ with particular pulses of sea-level rise or fall. Further high-resolution case studies need to be accompanied by more advanced numerical modelling in order to understand more fully the relationships between orbital forcing, Cretaceous climate, sea level and the carbon cycle.

Acknowledgements

This research was supported by the Czech Science Foundation (GACR) grant P210/10/1991 to DU. DRG and IJ acknowledge funding by UK Natural Environment Research Council (NERC) grants NE/H020756/1 and NE/H021868/1. KO was supported by Statoil Petroleum AS contract 4501936147. Additional analytical work was funded by Czech Ministry of Education Project LA08036, led by A. Špičák. DU and JL acknowledge support from research programme AV0Z30120515 of the Academy of Sciences of the Czech Republic.

References

Ando, A., Huber, B.T., MacLeod, K.G., Ohta, T., Khim, B.-K., 2009. Blake Nose stable isotopic evidence against the mid-Cenomanian glaciation hypothesis. Geology 37, 451–454. doi:10.1130/G25580A.1.

Arthur, M.A., Dean, W.E., Pratt, L.M., 1988. Geochemical and climatic effects of increased marine organic carbon burial at the Cenomanian/Turonian boundary. Nature 335, 714-717. doi:10.1038/335714a0.

Bice, K.L., Huber, B.T., Norris, R.D., 2003. Extreme polar warmth during the Cretaceous greenhouse? Paradox of the late Turonian $\delta^{18}O$ record at Deep Sea Drilling Project Site 511. Paleoceanography 18. doi: 10.1029/2002PA000848.

Bjerrum, C.J., Bendtsen, J., Legarth, J.J.F., 2006. Modeling organic carbon burial during sea level rise with reference to the Cretaceous. Geochem. Geophys. Geosyst. 7. Q05008, doi:10.1029/2005GC001032.

Bornemann, A., Norris, R.D., Friedrich, O., Beckmann, B., Schouten, S., Damste, J.S.S., Vogel, J., Hofmann, P., Wagner, T., 2008. Isotopic evidence for glaciation during the Cretaceous supergreenhouse. Science 319, 189-192.

Boulila, S., Galbrun, B., Miller, K.G., Pekar, S.F., Browning, J.V., Laskar, J., Wright, J.D., 2011. On the origin of Cenozoic and Mesozoic "third-order" eustatic sequences. Earth-Sci. Rev. 109, 94-112.

Boulila, S., Galbrun, B., Laskar, J., Palike, H., 2012. A similar to 9 myr cycle in Cenozoic $\delta^{13}C$ record and long-term orbital eccentricity modulation: Is there a link? Earth Planet. Sci. Lett. 317: 273-281.

Burnett, J.A., 1998. Upper Cretaceous. In: Bown, P.R. (Ed.), Calcareous Nannofossil Biostratigraphy. Chapman and Hall, London, pp. 132–199.

Burton, R., Kendall, C.G.St.C., Lerche, I., 1987. Out of our depth: on the impossibility of fathoming eustasy from the stratigraphic record. Earth Sc. Rev. 24, 237-277.

Cramer, B.S., Wright, J.D., Kent, D.V., Aubry, M.-P. 2003. Orbital climate forcing of $\delta^{13}C$ excursions in the late Paleocene–early Eocene (chrons C24n–C25n). Paleoceanography, 18, 1097. doi:10.1029/2003PA000909.

Čech, S., 1989. Upper Cretaceous *Didymotis* Events from Bohemia. In: Wiedmann, J (Ed.), Cretaceous of the Western Tethys, Proceedings of the 3rd International Cretaceous Symposium, Tübingen 1987, pp. 657-676. E. Schweizerbart, Stuttgart.

Čech, S., Klein, V., Kříž, J., Valečka, J., 1980. Revision of the Upper Cretaceous stratigraphy of the Bohemian Cretaceous Basin. Věstník Ústředního Ústavu geologického 55, 277-296.

Čech, S., Rejchrt, M., Štaffen, Z., 2011. Křídové sedimenty ve vrtu V 800 Střeleč, jejich petrografie, litostratigrafie a chemostratigrafie. – Zprávy o geologických výzkumech v roce 2010 44, 14-19 (with English summary).

Dercourt, J., Gaetani, M., Vrielynck, B., Barrier, E., Biju-Duval, B., Brunet, M.F., Cadet, J.P., Crasquin, S., Snadulescu, M. (Eds), 2000. Atlas Peri-Tethys, Palaeogeographical Maps. CCGM/CGMW, Paris: 24 maps and explanatory notes: I-XX, 269 pp.

Dewey, J.F., Pitman, W.C., 1998. Sea-level changes: mechanisms, magnitudes and rates. In: Pindell, J.L., Drake, C. (Eds), Paleogeographic Evolution and Non-glacial Eustasy, Northern South America. SEPM Spec. Publ. 58, 1-16.

Embry, A.F., 1995. Sequence boundaries and sequence heirarchies: problems and proposals. In: Steel, R.J., Felt, V.L., Johannesson, E.P., Mathieu C. (Eds), Sequence Stratigraphy on the Northwest European Margin. Norwegian Petroleum Soc. Spec. Publ. 5, 1-11.

Flögel, S., Wallmann, K., Kuhnt, W., 2011. Cool episodes in the Cretaceous - Exploring the effects of physical forcings on Antarctic snow accumulation. Earth Planet. Sci. Lett. 307, 279-288.

Friedrich, O., Norris, R.D., Erbacher, J., 2012. Evolution of middle to Late Cretaceous oceans - A 55 m.y. record of Earth's temperature and carbon cycle. Geology, 40, 107-110.

Galloway, W.E., 1989. Genetic stratigraphic sequences in basin analysis I: Architecture and genesis of flooding-surface bounded depositional units. AAPG Bull. 73, 125-142.

Gale, A.S., 1996. Turonian correlation and sequence stratigraphy of the Chalk in southern England. In: Hesselbo, S.P., Parkinson D.N. (Eds), Sequence Stratigraphy in British Geology. Geol. Soc. London Spec. Publ. 103, 177–195.

Gale, A.S., Jenkyns, H.C., Kennedy, W.J., Corfield, R.M., 1993. Chemostratigraphy versus biostratigraphy: data from around the Cenomanian–Turonian boundary. J. Geol. Soc. London 150, 29–32.

Gardner, M.H., 1995. The stratigraphic hierarchy and tectonic history of the mid-Cretaceous foreland basin of central Utah. In: Dorobek, S.L., Ross G.M. (Eds), Stratigraphic Evolution of Foreland Basins, SEPM Spec. Publ. 52, 283-303.

Giorgioni, M., Weissert, H., Bernasconi, S.M., Hochuli, P.A., Coccioni, R., Keller, C.E., 2012. Orbital control on carbon cycle and oceanography in the mid-Cretaceous greenhouse. Paleoceanography, 27, PA1204, doi:10.1029/2011PA002163.

Gröcke, D.R., 2002. The carbon isotope composition of ancient CO_2 based on higher-plant organic matter. Phil. Trans. Roy. Soc. London Ser. A – Math. Phys. Eng. Sci. 360, 633-658.

Gröcke, D.R., Hesselbo, S.P., Jenkyns, H.C., 1999. Carbon-isotope composition of Lower Cretaceous fossil wood: Ocean-atmosphere chemistry and relation to sea-level change. Geology 27, 155-158.

Gröcke, D.R., Ludvigson, G.A., Witzke, B.L., Robinson, S.A., Joeckel, R.M., Ufnar, D.F., Ravn, R.L., 2006. Recognizing the Albian-Cenomanian (OAE1d) sequence boundary using plant carbon isotopes: Dakota Formation, Western Interior Basin, USA. Geology 34, 193-196.

Hancock, J.M., Kauffman, E.G., 1979. The great transgressions of the Late Cretaceous. J. Geol. Soc. London 136, 175-186.

Haq, B.U., Hardenbol, J., Vail, P.R., 1988. Mesozoic and Cenozoic chronostratigraphy and eustatic cycles. In: Wilgus, C.K., Hastings, B.S., Kendall, C.G.St.C., Posamentier, H.W., Ross, C.A., Van Wagoner, J.C. (Eds), Sea Level Changes: An Integrated Approach. SEPM Spec. Publ. 42, 71-109.

Hayes, J.M, Popp, B.N., Takigiku, R., Johnson, M.W., 1989. An isotopic study of biogeochemical relationships between carbonates and organic carbon in the Greenhorn Formation. Geochim. Cosmochim. Acta 53, 2961–2972.

Herrle, J.O., Kossler, P., Friedrich, O., Erlenkeuser, H., Hemleben, C., 2004. High-resolution carbon isotope records of the Aptian to Lower Albian from SE France and the Mazagan Plateau (DSDP Site 545): a stratigraphic tool for paleoceanographic and paleobiologic reconstruction. Earth Planet. Sci. Lett. 218, 149-161.

Hesselbo, S.P., Pienkowski, G., 2011. Stepwise atmospheric carbon-isotope excursion during the Toarcian Oceanic Anoxic Event (Early Jurassic, Polish Basin). Earth Planet. Sci. Lett. 301, 365-372.

Immenhauser, A., 2005. High-rate sea-level change during the Mesozoic: New approaches to an old problem. Sedim. Geol. 175, 277-296.

Immenhauser, A, Matthews, R.K., 2004. Albian sea-level cycles in Oman: the "Rosetta Stone" approach. GeoArabia 9, 11– 46.

Jarvis, I., Murphy, A.M., Gale, A.S., 2001. Geochemistry of pelagic and hemipelagic carbonates: criteria for identifying systems tracts and sea-level change. J. Geol. Soc. London 158, 685-696.

Jarvis, I., Mabrouk, A., Moody, R.T.J., de Cabrera, S., 2002. Late Cretaceous (Campanian) carbon isotope events, sea-level change and correlation of the Tethyan and Boreal realms. Palaeogeog. Palaeoclimatol. Palaeoecol. 188, 215-248.

Jarvis, I., Gale, A.S., Jenkyns, H.C., Pearce, M.A., 2006. Secular variation in Late Cretaceous carbon isotopes: a new $\delta^{13}C$ carbonate reference curve for the Cenomanian-Campanian (99.6-70.6 Ma). Geol. Mag. 143, 561-608.

Jarvis, I., Lignum, J.S., Gröcke, D.R., Jenkyns, H.C., Pearce, M.A., 2011. Black shale deposition, atmospheric CO_2 drawdown, and cooling during the Cenomanian-Turonian Oceanic Anoxic Event. Paleoceanography 26. doi: 10.1029/2010pa002081.

Jenkyns, H.C., Gale, A.S., Corfield, R.M., 1994. Carbon-isotope and oxygen-isotope stratigraphy of the English Chalk and Italian Scaglia and its palaeoclimatic significance. Geol. Mag. 131, 1-34.

Kauffman, E.G. and Caldwell, W.G.E., 1993. The Western Interior Basin in space and time. In: Evolution of the Western Interior Basin (Eds. W.G.E. Caldwell, and E.G. Kauffmann), Geol. Assoc. Canada Spec. Paper, 39, 1-30.

Klein, V., Müller, V., Valečka, J., 1979. Lithofazielle und paläogeographische Entwicklung des Böhmischen Kreidebeckens. Aspekte der Kreide Europas. IUGS Series A 6, 435-446.

Klein, V., Hercogová, J., Rejchrt, M. 1982. Stratigraphie, lithologie und paläontologie der Kreide im Elbe-Faziesgebiet. Sborník geologických věd Geologie 36, 27-92.

Kominz, M.A., Browning, J.V., Miller, K.G., Sugarman, P.J., Mizintseva, S., Scotese, C.R., 2008. Late Cretaceous to Miocene sea-level estimates from the New Jersey and Delaware coastal plain coreholes: an error analysis. Basin Res. 20, 211-226.

Kump, L.R., Arthur, M.A., 1999. Interpreting carbon-isotope excursions: carbonates and organic matter. Chem. Geol. 161, 181-198.

Laurin, J., Sageman, B.B., 2007. Cenomanian–Turonian coastal record in SW Utah, U.S.A.: Orbital-scale transgressive–regressive events during Oceanic Anoxic Event II. J. Sedim. Res. 77, 731–756.

Laurin, J., Uličný, D., 2004. Controls on a shallow-water hemipelagic carbonate system adjacent to a siliciclastic margin: Example from late Turonian of Central Europe. J. Sedim. Res. 74, 697-717.

Lees, J.A., 2008. The calcareous nannofossil record across the Late Cretaceous Turonian/ Coniacian boundary, including new data from Germany, Poland, the Czech Republic and England. Cretaceous Res. 29, 40–64.

Meyers, P.A., 1997. Organic geochemical proxies of paleoceanographic, paleolimnologic, and paleoclimatic processes. Org. Geochem. 27, 213-250.

Miller, K.G., Sugarman, P.J., Browning, J.V., Kominz, M.A., Hernandez, J.C., Olsson, R.K., Wright, J.D., Feigenson, M.D., Van Sickel, W., 2003. Late Cretaceous chronology of large, rapid sea-level changes: Glacioeustasy during the greenhouse world. Geology 31, 585-588.

Miller, K.G., Kominz, M.A., Browning, J.V., Wright, J.D., Mountain, G.S., Katz, M.E., Sugarman, P.J., Cramer, B.S., Christie-Blick, N., Pekar, S.F., 2005. The Phanerozoic record of global sea-level change. Science 310, 1293-1298.

Miller, K.G., Mountain, G.S., Wright, J.D., Browning, J.V., 2011. A 180-million-year record of sea level and ice volume variations from continental margin and deep-sea isotopic records. Oceanography 24, 40-53.

Mitchell, A., Uličný, D., Hampson, G.J., Allison, P.A., Gorman, G.J., Piggott, M.D., Wells, M.R., Pain, C.C., 2010. Modelling tidal current-induced bed shear stress and palaeocirculation in an epicontinental seaway: the Bohemian Cretaceous Basin, Central Europe. Sedimentology 57, 359-388. doi: 10.1111/j.1365-3091.2009.01082.x.

Mitchell, S.F., Paul, C.R.C., Gale, A.S., 1996. Carbon isotopes and sequence stratigraphy. In: Howell, J.A., Aitken J.F. (Eds), High-resolution Sequence Stratigraphy: Innovations and Applications. Geol. Soc. Spec. Publ. 104, 11-24.

Moriya, K., Wilson, P.A., Friedrich, O., Erbacher, J., Kawahata, H., 2007. Testing for ice sheets during the mid-Cretaceous greenhouse using glassy foraminiferal calcite from the mid-Cenomanian tropics on Demerara Rise. Geology, 35, 615-618.

Olszewska-Nejbert, D., 2004. Development of the Turonian/Coniacian hardground boundary in the Cracow Swell area (Wielkanoc quarry, Southern Poland). Geol. Q. 48, 159–170.

Ogg, J.G., Hinnov, L.A., 2012. Cretaceous. In: Gradstein, F.M. Ogg, M.J., Schmitz, G., Ogg, G. (Eds), The Geologic Time Scale 2012, pp. 793-853. Elsevier, Amsterdam. doi: 10.1016/B978-0-444-59425-9.00027-5.

Pälike, H., Norris, R.D., Herrle, J.O., Wilson, P.A., Coxall, H.K., Lear, C.H., Shackleton, N.J., Tripati, A.K., Wade B.S., 2006. The heartbeat of the Oligocene climate system. Science 314, 1894–1898. doi:10.1126/science.1133822.

Plint, A.G., 1991, High-frequency relative sea-level oscillations in the Upper Cretaceous shelf clastics of the Alberta foreland basin: possible evidence for a glacio-eustatic control. In: McDonald, D.I.M. (Ed.), Sedimentation, Tectonics and Eustasy. Internat. Assoc. Sedimentol. Spec. Publ. 12, 409–428.

Popp, B.N., Tsakigiku, R.T., Hayes, J.M., Louda, J.W., Baker, E.W., 1988. The post-Paleozoic chronology and mechanism of ^{13}C depletion in primary marine organic matter. Am. J. Sci. 289, 436-454.

Richardt, N., Wilmsen, M., 2012. Lower Upper Cretaceous standard section of the southern Münsterland (NW Germany): carbon stable-isotopes and sequence stratigraphy. Newslett. Stratigr. 45, 1–24.

Sahagian, D.L., Beisel, A.L., Zakharov, V.A., 1994. Sequence stratigraphic enhancement of biostratigraphic correlation with application to the Upper Cretaceous of northern Siberia: a potential tool for petroleum exploration. Geol. Rev. 36, 359–372.

Sahagian, D.L., Pinous, O., Olferiev, A., Zakharov, V., 1996. Eustatic curve for the Middle Jurassic-Cretaceous based on Russian platform and Siberian stratigraphy: Zonal resolution. AAPG Bull. 80, 1433-1458.

Scholle, P.A., Arthur, M.A., 1980. Carbon isotope fluctuations in Cretaceous pelagic limestones - potential stratigraphic and petroleum-exploration tool. AAPG Bull. 64, 67-87.

Shank, J.A., Plint, A.G., in press: Allostratigraphy of the Upper Cretaceous Cardium Formation in subsurface and outcrop in southern Alberta, and correlation to equivalent

strata in northwestern Montana. Bull. Can. Petrol. Geol. Accepted ms. BCPG-D-12-00024R1.

Siegenthaler, U., Sarmiento, J., 1993. Atmospheric carbon dioxide and the ocean. Nature, 365, 119– 125.

Sømme T.O., Helland-Hansen W., Granjeon D., 2009b, Impact of eustatic amplitude variations on shelf morphology, sediment dispersal, and sequence stratigraphic interpretation: Icehouse versus greenhouse systems. Geology, 37, 587–590. doi: 10.1130/G25511A.1.

Sprovieri, M., Sabatino, N., Pelosi, N., Batenburg, S.J., Coccioni, R., Iavarone, M., Mazzola, S., 2013. Late Cretaceous orbitally-paced carbon isotope stratigraphy from the Bottaccione Gorge (Italy). Palaeogeography, Palaeoclimatology, Palaeoecology, 379–380, 1–94.

Stoll, H.M., Schrag, D.P., 2000. High-resolution stable isotope records from the Upper Cretaceous rocks of Italy and Spain: Glacial episodes in a greenhouse planet? Geol. Soc. Am. Bull. 112, 308-319.

Sugarman, P.J., Miller, K.G., Olsson, R.K., Browning, J.V., Wright, J.D., De Romero, L.M., White, T.S., Muller, F.L., Uptegrove, J., 1999. The Cenomanian/Turonian carbon burial event, Bass River, NJ, USA: Geochemical, paleoecological, and sea-level changes. J. Foram. Res. 29, 438-452.

Swenson, J. B., Muto, T., 2007. Response of coastal plain rivers to falling relative sea-level: allogenic controls on the aggradational phase. Sedimentology 54, 207-221.

Takashima, R., Nishi, H., Yamanaka, T., Hayashi, K., Waseda, A., Obuse, A., Tomosugi, T., Deguchi, N., Mochizuki, S., 2010. High-resolution terrestrial carbon isotope and planktic foraminiferal records of the Upper Cenomanian to the Lower Campanian in the Northwest Pacific. Earth. Planet. Sci. Lett. 289, 570-582.

Takashima, R., Nishi, H., Yamanaka, T., Tomosugi, T., Fernando, A.G., Tanabe, K., Moriya, K., Kawabe, F., Hayashi, K., 2011. Prevailing oxic environments in the Pacific Ocean during the mid-Cretaceous Oceanic Anoxic Event 2. Nature Comm. 2. doi: 10.1038/ncomms1233.

Uličný, D., 2001. Depositional systems and sequence stratigraphy of coarse-grained deltas in a shallow-marine, strike-slip setting: the Bohemian Cretaceous Basin, Czech Republic. Sedimentology 48, 599-628.

Uličný, D., Hladíková, J., Hradecká, L., 1993. Record of sea-level changes, oxygen depletion and the $\delta^{13}C$ anomaly across the Cenomanian-Turonian boundary, Bohemian Cretaceous Basin. Cretaceous Res. 14, 211-234.

Uličný, D., Hladíková, J., Attrep, M., Čech, S., Hradecká, L., Svobodová, M., 1997. Sea-level changes and geochemical anomalies across the Cenomanian-Turonian boundary: Pecínov quarry, Bohemia. Palaeogeog. Palaeoclimatol. Palaeoecol. 132, 265-285.

Uličný, D., Laurin, J., Čech, S., 2009. Controls on clastic sequence geometries in a shallow-marine, transtensional basin: the Bohemian Cretaceous Basin, Czech Republic. Sedimentology 56, 1077–1114. doi: 10.1111/j.1365-3091.2008.01021.x

Varban, B.L., Plint, A.G., 2008. Sequence stacking patterns in the Western Canada foredeep: influence of tectonics, sediment loading and eustasy on deposition of the Upper Cretaceous Kaskapau and Cardium Formations. Sedimentology 55, 395-421.

Voigt, S., 2000. Cenomanian–Turonian composite $\delta^{13}C$ curve for Western and Central Europe: the role of organic and inorganic carbon fluxes. Palaeogeog. Palaeoclimatol. Palaeoecol. 160, 91–104.

Voigt, S., Wiese, F., 2000. Evidence for Late Cretaceous (Late Turonian) climate cooling from oxygen-isotope variations and palaeobiogeographic changes in Western and Central Europe. J. Geol. Soc. London 157, 737-743.

Voigt, S., Aurag, A., Leis, F., Kaplan, U., 2007. Late Cenomanian to Middle Turonian high-resolution carbon isotope stratigraphy: New data from the Münsterland Cretaceous Basin, Germany. Earth Planet. Sci. Lett. 253, 196-210.

Voigt, S., Erbacher, J., Mutterlose, J., Weiss, W., Westerhold, T., Wiese, F., Wilmsen, M., Wonik, T., 2008a. The Cenomanian-Turonian of the Wunstorf section (North Germany): global stratigraphic reference section and new orbital time scale for Oceanic Anoxic Event 2. Newslett. Stratigr. 43, 65-89.

Voigt, S., Wagreich, M., Surlyk, F., Walaszczyk, I., Uličný, D. Čech, S., Voigt, T., Wiese, F., Wilmsen, M., Niebuhr, B., Reich, M., Funk, H., Michalík, J., Jagt., J.W.M., Felder, P.J., Schulp A.S., 2008b: Cretaceous. In: McCann, T. (Ed.), Geology of Central Europe, Volume 2: Mesozoic and Cenozoic, pp. 923-997. The Geological Society, London.

Walaszcyk, I., Shank, J.A., Plint, A.G., Cobban, W.A., in revision. Hiatuses in the lower Niobrara Formation of the central US Western Interior Basin revealed by inoceramid faunal succession in the Cardium Formation, Alberta. GSA Bull. (acceptance expected early 2013).

Wendler, I., Willems, H., Grafe, K.U., Ding, L., Luo, H., 2011. Upper Cretaceous inter-hemispheric correlation between the Southern Tethys and the Boreal: chemo- and biostratigraphy and paleoclimatic reconstructions from a new section in the Tethys Himalaya, S-Tibet. Newslett. Stratigr. 44, 137-171.

Wiese, F., Kröger, B., 1998. Evidence for a shallowing event in the Upper Turonian (Cretaceous) *Mytiloides scupini* Zone of northern Germany. Acta Geol. Polon. 48, 3, 265-284.

Wiese, F., Voigt, S., 2002. Late Turonian (Cretaceous) climate cooling in Europe: faunal response and possible causes. Geobios, 35, 65-77.

Wiese, F., Čech, S., Ekrt, B., Košťák, M., Mazuch, M., Voigt, S., 2004. The Upper Turonian of the Bohemian Cretaceous Basin (Czech Republic) exemplified by the Upohlavy working quarry: integrated stratigraphy and palaeoceanography of a gateway to the Tethys. Cretaceous Res. 25, 329-352.

Zhu, Y.J., Bhattacharya, J.P., Li, W.G., Lapen, T.J., Jicha, B.R., Singer, B.S., 2012. Milankovitch-scale sequence stratigraphy and stepped forced regressions of the Turonian Ferron Notom deltaic complex, south-central Utah, USA. J. Sedim. Res. 82, 723-746.

Ziegler, P. A., 1990. Geological Atlas of Western and Central Europe. pp. 1-239. Shell Internationale Petroleum Maatschappij, The Hague.

FIGURE CAPTIONS

Fig. 1. Geological setting of the study area. A. A simplified palaeogeography of the European epicontinental sea showing the location of the Bch-1 well and other sections discussed in text. Adapted from Mitchell et al. (2010) and references therein, mainly Ziegler (1990) and Dercourt et al. (2000). B. Detail of the Bohemian Cretaceous Basin (BCB). Location indicated by rectangle in A. Main clastic source areas and sub-basins are shown: NW, Lužice-Jizera sub-basin; SE, Orlice-Žďár sub-basin. TUR 2, 4 ... CON 1 indicate regressive limits of nearshore strata in genetic sequences (see text and Figs 2, 4). Figure S1 in Supplementary Materials shows details of stratigraphic correlation panel along the line shown.

Fig. 2. Bch-1 core: biostratigraphic data, lithology, elemental and palynological proxy parameters, TOC contents, and $\delta^{13}C_{org}$ curve correlated to the T-Rmax (shore proximity) curves of the SE and NW sub-basins, and an inferred sea-level curve. Main regional tectonic events affecting the T-R history in both sub-basins are shown. Details in text.

Fig. 3. Correlation of $\delta^{13}C_{org}$ and biostratigraphic data from Bch-1 to the Chalk reference curve and other high-resolution $\delta^{13}C_{carb}$ records (location of sections in Fig. 1). Correlation datum is the level of the Navigation Carbon Isotope Event. The base of the Coniacian in Bch-1 , based on the inferred FO *C. deformis erectus*, is placed at the Navigation $\delta^{13}C_{org}$ minimum. The faunal assemblage of the *Micraster* marl in Salzgitter is considered equivalent to the *M. scupini* acme event in Bch-1.

Fig. 4. A comparison of the inferred sea-level fluctuations based on the Bohemian Cretaceous T-R history and the $\delta^{13}C_{org}$ record, with published estimates of Turonian sea-level changes based on lower-resolution datasets. Note that the beginning of the Apulian platform hiatus / LST has two alternatives in dating. Details in text.

SUPPLEMENTARY MATERIALS

Uličný et al.: Carbon-Isotope Record of the Turonian Stage (93.9 – 89.8 Ma)....

Figure S1. A representative correlation panel showing an example of chronostratigraphic relationships between the Bch-1 core and the infills of the two main sub-basins of the Bohemian Cretaceous Basin. The panel is divided into a northwestern part (the Lužice-Jizera sub-basin, A) and a southeastern part (the Orlice-Žďár sub-basin, B). For location of the correlation line see inset maps. The correlations are based on a three-dimensional network of c. 700 well-logs and cored boreholes, supplemented by outcrop data (updated from Uličný et al., 2009). Where available, biostratigraphic datums indentified in cored boreholes are included. Colour infills characterize sandstone-dominated facies of individual genetic sequences TUR 1- CON 2. Correlation datums float within the panels in order to prevent unrealistic the effects of syndepositional deformation. To save space, wells are plotted equidistantly, therefore the vertical exaggeration varies within panels. Cenomanian strata and strata younger than CON 2 are not differentiated. See Data and Methods for further details.

Figure S2. Bch-1 core: elemental ratios (Si/Al, Zr/Al and Ti/Al) discussed in the text, n-alkane-based terrestrial-aquatic ratio, and CaCO3 contents. Biostratigraphy, lithology, T:M palynomorph ratio and $\delta^{13}C_{org}$ curve shown for reference. Genetic sequences TUR1 through CON 2 are indicated. Note that of the 14 samples analyzed for n-alkane ratios, only one shows a higher TAR value than 0.7. Comments in text,

Table ST1. Carbon-isotope composition of bulk organic matter and total organic carbon contents in the insoluble residue; Bch-1 core.

Table ST2. Selected element concentrations and element ratios; Bch-1 core.

Table ST3. Terrestrial to aquatic ratio (TAR) of organic matter based on n-alkane analyses.Comments in text.

Appendix 1.

A. Bch-1 well coordinates

N 50°18´54.2´´
E 15°17´42.03´´

B. laboratory procedures

To be supplied by co-authors

d13Corg - JTA

elemental analyses – IJ, CaCO3 calculation

N-alkane analysis, terrestrial-aquatic proxy calculation

Powdered rock samples were extracted with dichloromethane using ASE 300 Accelerated Solvent Extraction System at 125 °C, 1,500 p.s.i. for 25 min. The total lipid fraction was analysed on an HP Agilent 7820A gas chromatographer (Agilent Technologies Inc., Wilmington, USA) equipped with a flame ionisation detector (FID). Helium was used as the carrier gas at a flow rate of 1.2 mL/min. Separation of organic compounds in the total lipid fraction was achieved using a DB-5 capillary column (30 m x 0.32 mm x 0.25 µm) (Agilent Technologies Inc., Santa Clara, USA). The GC oven was programmed from 50 °C (1 min) at 20 °C/min to 150 °C and at 8 °C/min to 320 °C (10 min). Samples were injected in a splitless mode. *n*-Alkanes were identified through comparison of elution times with those of *n*-alkanes in a standard containing *n*-C_{16} to *n*-C_{30} alkanes. The $(nC_{17}+nC_{19})/(nC_{29}+nC_{31})$ alkane ratio was calculated using *n*-alkane peak areas.

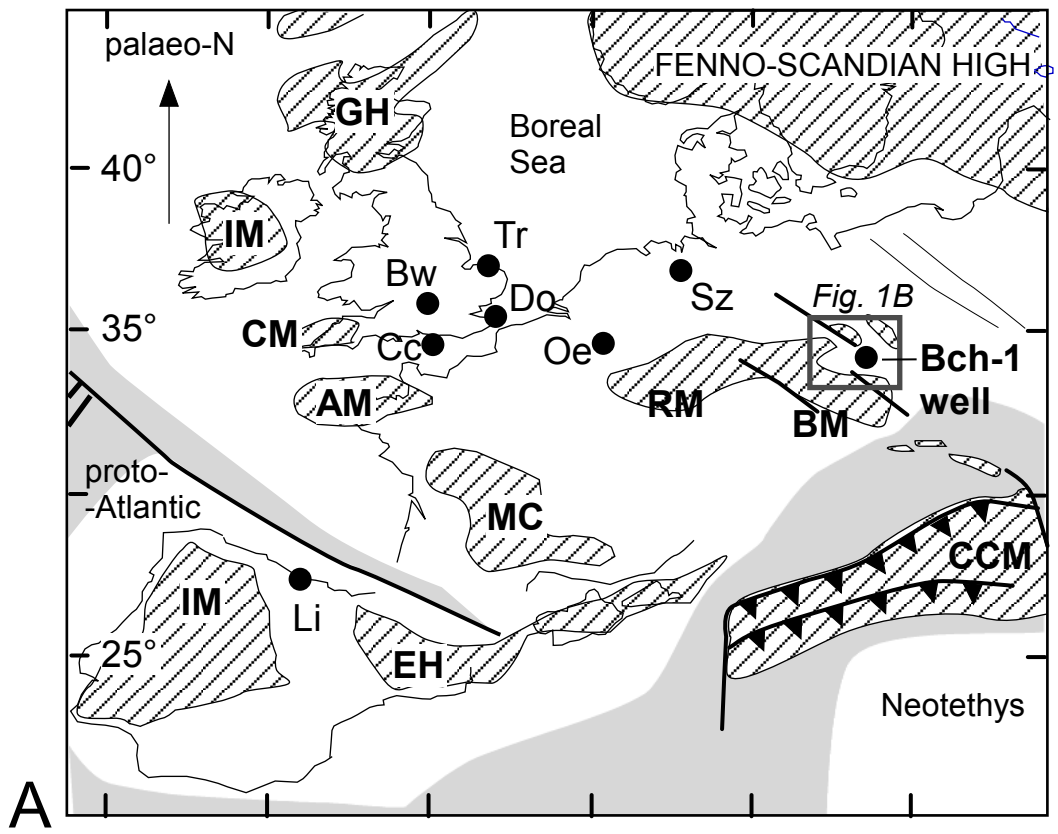

emerged highs

shallow epicontinental sea

deep marine settings

Emerged landmasses: AM- Armorican Massif, MC - Massif Central, RM - Rhenish, BM - Bohemian Massif, IM - Irish massif, GH - Grampian High, EH - Ebro High, IM - Iberian Massif.

Oe● Localities with carbon-isotope data correlated in Fig. 3:

Sz - Salzgitter-Salder, Oe - Oerlinghausen, Li - Liencres; main parts of Chalk composite isotope curve: Bw - Banterwick, Tr - Trunch, Cc - Culver Cliff, Do - Dover

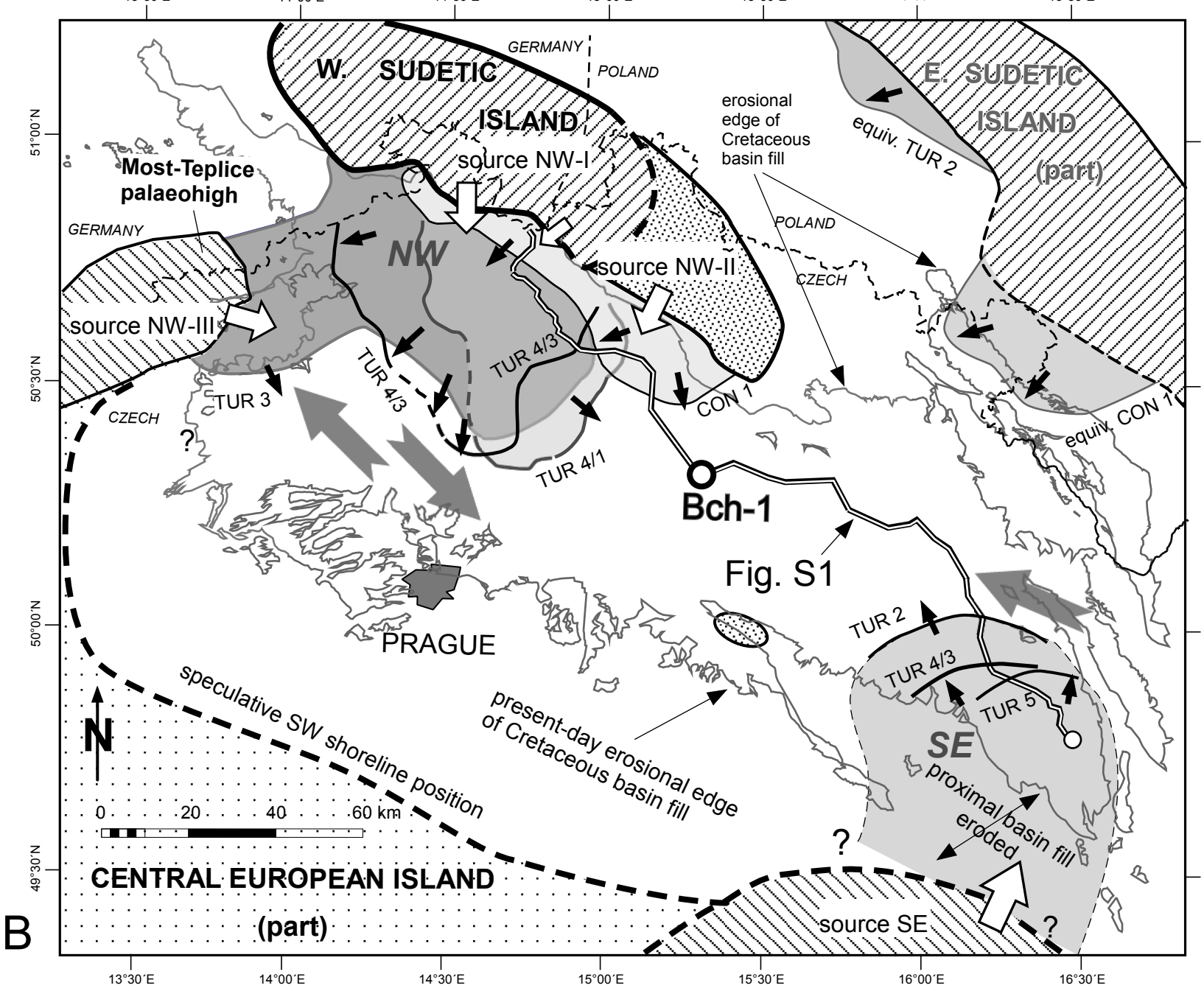

state border

tectonically inactive emerged land

source areas

extent of regressive facies (deltaic / shoreface)

offshore facies

limit of maximum regression & progradation direction

clastic input direction

palaeocurrent direction

○ TO-1 borehole shown in Fig. S1

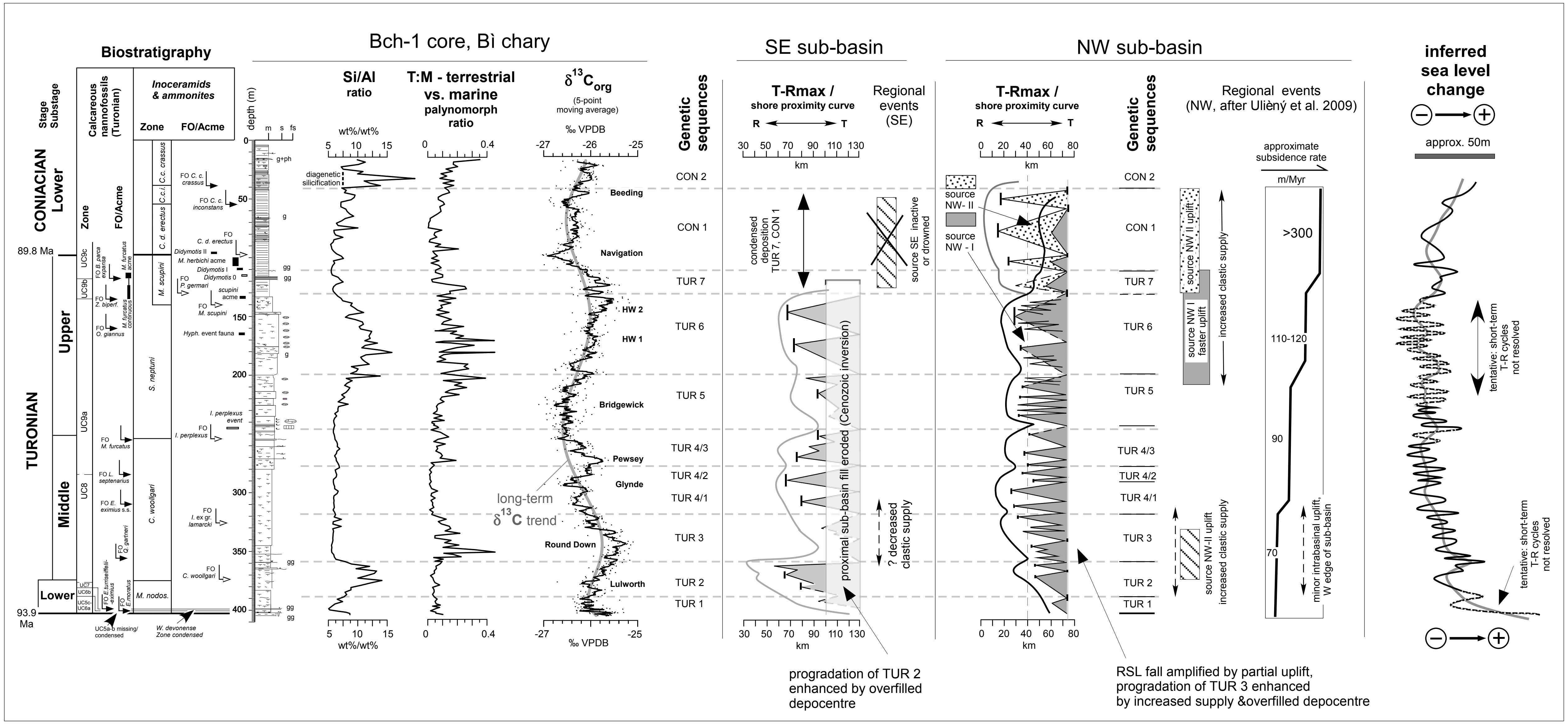

Biostratigraphy
Bch-1 core, Bì chary
SE sub-basin
NW sub-basin
inferred sea level change
Stage Substage
Calcareous nannofossils (Turonian)
Zone
FO/Acme
Inoceramids & ammonites
CONIACIAN Lower
TURONIAN
Upper
Middle
Lower
89.8 Ma
93.9 Ma
depth (m)
Si/Al ratio
wt%/wt%
T:M - terrestrial vs. marine palynomorph ratio
δ13Corg (5-point moving average)
‰ VPDB
diagenetic silicification
Beeding
Navigation
HW 2
HW 1
Bridgewick
Pewsey
Glynde
Round Down
Lulworth
long-term δ13C trend
Genetic sequences
CON 2
CON 1
TUR 7
TUR 6
TUR 5
TUR 4/3
TUR 4/2
TUR 4/1
TUR 3
TUR 2
TUR 1
T-Rmax / shore proximity curve
R T
km
Regional events (SE)
condensed deposition TUR 7, CON 1
source SE inactive or drowned
proximal sub-basin fill eroded (Cenozoic inversion)
? decreased clastic supply
progradation of TUR 2 enhanced by overfilled depocentre
source NW- II
source NW - I
Regional events (NW, after Uličný et al. 2009)
source NW II uplift
source NW I faster uplift
increased clastic supply
source NW-II uplift increased clastic supply
approximate subsidence rate
m/Myr
>300
110-120
90
70
minor intrabasinal uplift, W edge of sub-basin
RSL fall amplified by partial uplift, progradation of TUR 3 enhanced by increased supply &overfilled depocentre
approx. 50m
tentative: short-term T-R cycles not resolved
UC5a-b missing/ condensed
W. devonense Zone condensed

English Chalk reference curve
(Jarvis et al. 2006, adjusted to GTS 2012)

Bch-1 Bì chary
(this study)

Liencres
(Wiese 1999)

Salzgitter-Salder,
(Voigt & Hilbrecht, 1997)

CONIACIAN
TURONIAN
CENOMANIAN
Lower
Middle
Upper
S. neptuni
C woollgari
M. nodos.
W. devonense
M. scup.
89.8 Ma
93.9 Ma
GTS (2012)
89
90
91
92
93
94
Ma
δ13Ccarb
δ13Corg
Light Point
Beeding
Navigation
Hitch Wood
Bridgewick
Caburn
Upper Southerham
Lower Southerham
'Pewsey'
"g1"
Glynde
"f1"
Tu11
Low-woollgari Tu10
Round Down Tu8
Lulworth Tu5
Holywell Tu1
OAE II CIE
FO M. scupini
FO S. neptuni
FO I. lamarcki
FO C. woollgari
FO M. geslinianum
FO C. c. crassus
FO C. c. inconstans
FO C. deformis erectus
Didymotis II
herbichi acme
Didymotis I
Didymotis 0
HW 3
M. scupini acme
FO P. germari
HW 2
FO M. scupini
Hyph. event fauna
HW 1
"h4"?
"h3"?
perplexus event
FO I. perplexus
Tu3
FO C. woollgari
FO I. cuvieri
‰ PDB
‰ VPDB
5 pt. moving average
meters
Peak +3
Peak +2
S. plana event
Micraster marl
Hitch Wood=Peak+1
Hyphantoceras event
costellatus/plana event
U.Sh.
L.Sh.
FO C. w. waltersdorfensis
FO C. deformis erectus
M. herbichi
Low-woollgarii Tu10
C.c. inconstans
C. d. erect.
M. scupini
I. perplexus
I. lamarcki
C. woollgari
M. nod.
W.d.
CEN.
correlation CIE
Lulworth Tu5 named CIE
FO C. woollgari index fossil first occurrence
I. perplexus event bioevent / acme
Oerlinghausen & Halle
(Voigt et al, 2007)

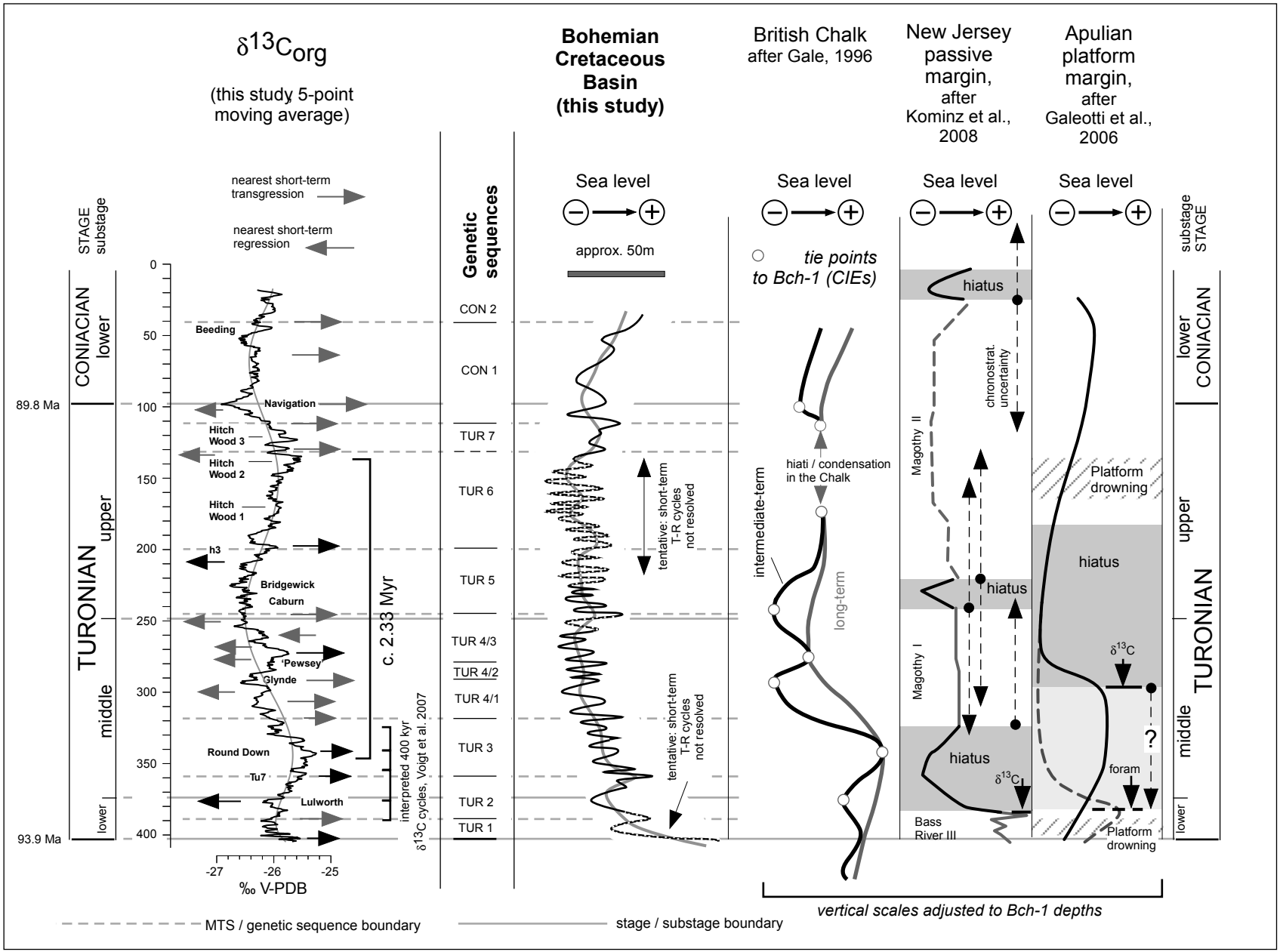
δ13Corg
(this study, 5-point moving average)
Bohemian Cretaceous Basin (this study)
British Chalk after Gale, 1996
New Jersey passive margin, after Kominz et al., 2008
Apulian platform margin, after Galeotti et al., 2006
nearest short-term transgression
nearest short-term regression
STAGE substage
Genetic sequences
Sea level
approx. 50m
tie points to Bch-1 (CIEs)
CONIACIAN lower
TURONIAN upper
middle
lower
89.8 Ma
93.9 Ma
Beeding
Navigation
Hitch Wood 3
Hitch Wood 2
Hitch Wood 1
h3
Bridgewick
Caburn
'Pewsey'
Glynde
Round Down
Tu7
Lulworth
c. 2.33 Myr
interpreted 400 kyr δ13C cycles, Voigt et al. 2007
CON 2
CON 1
TUR 7
TUR 6
TUR 5
TUR 4/3
TUR 4/2
TUR 4/1
TUR 3
TUR 2
TUR 1
tentative: short-term T-R cycles not resolved
hiati / condensation in the Chalk
intermediate-term
long-term
hiatus
chronostrat. uncertainty
Magothy II
Magothy I
δ13C
Bass River III
Platform drowning
foram
?
‰ V-PDB
MTS / genetic sequence boundary
stage / substage boundary
vertical scales adjusted to Bch-1 depths

Fig. 4